Overcoming undesirable hERG affinity by incorporating fluorine atoms: A case of MAO-B inhibitors derived from 1 H-pyrrolo-[3,2-c]quinolines

Katarzyna Grychowska, Agnieszka Olejarz-Maciej, Klaudia Blicharz, Wojciech Pietruś, Tadeusz Karcz, Rafal Kurczab, Paulina Koczurkiewicz, Agata Doroz-Plonka, Gniewomir Latacz, Abdul Raheem Keeri, et al.

European Journal of Medicinal Chemistry 236 (2022) 114329

Contents lists available at ScienceDirect

European Journal of Medicinal Chemistry

journal homepage: http://www.elsevier.com/locate/ejmech

Overcoming undesirable *h*ERG affinity by incorporating fluorine atoms: A case of MAO-B inhibitors derived from 1 *H*-pyrrolo-[3,2-*c*] quinolines

Katarzyna Grychowska [a, *], Agnieszka Olejarz-Maciej [a], Klaudia Blicharz [a], Wojciech Pietruś [b], Tadeusz Karcz [a], Rafał Kurczab [b], Paulina Koczurkiewicz [a], Agata Doroz-Płonka [a], Gniewomir Latacz [a], Abdul Raheem Keeri [a], Kamil Piska [a], Grzegorz Satała [b], Joanna Pęgiel [a], Wojciech Trybała [a], Magdalena Jastrzębska-Więsek [a], Andrzej J. Bojarski [b], Frédéric Lamaty [c], Anna Partyka [a], Maria Walczak [a], Martyna Krawczyk [b], Natalia Malikowska-Racia [b], Piotr Popik [b], Paweł Zajdel [a, **]

[a] *Faculty of Pharmacy Jagiellonian University Medical College, 9 Medyczna Str, 30-688, Kraków, Poland*
[b] *Maj Institute of Pharmacology, Polish Academy of Sciences, 12 Smętna Str, 31-324, Kraków, Poland*
[c] *IBMM, Université de Montpellier, CNRS, ENSCM, Montpellier, France*

ARTICLE INFO

Article history:
Received 27 January 2022
Received in revised form
24 March 2022
Accepted 26 March 2022

Keywords:
Alzheimer's disease
MAO-B inhibitors
Glia
Cognition
Fluorinated compounds
*h*ERG channel

ABSTRACT

The incorporation of the fluorine motif is a strategy widely applied in drug design for modulating the activity, physicochemical parameters, and metabolic stability of chemical compounds. In this study, we attempted to reduce the affinity for ether-à-go-go-related gene (*h*ERG) channel by introducing fluorine atoms in a group of 1*H*-pyrrolo[3,2-*c*]quinolines that are capable of inhibiting monoamine oxidase type B (MAO-B). A series of structural modifications guided by *in vitro* evaluation of MAO-B inhibition and antitargeting for *h*ERG channels were performed, which led to the identification of 1-(3-chlorobenzyl)-4-(4,4-difluoropiperidin-1-yl)-1*H*-pyrrolo[3,2-*c*]quinoline (**26**). Compound **26** acted as a reversible MAO-B inhibitor exhibiting selectivity over 45 targets, enzymes, transporters, and ion channels, and showed potent glioprotective properties in cultured astrocytes. In addition, the compound demonstrated good metabolic stability in rat liver microsomes assay, a favorable safety profile, and brain permeability. It also displayed procognitive effects in the novel object recognition test in rats and antidepressant-like activity in forced swim test in mice. The findings of the study suggest that reversible MAO-B inhibitors can have potential therapeutic applications in Alzheimer's disease.

1. Introduction

Alzheimer's disease (AD), a severe neurodegenerative disorder, which constitutes the most common form of dementia, is becoming more common, posing a significant burden on public health. The currently available pharmacotherapy for AD mainly involves symptomatic treatment. Although the recent approval of Aducanumab, a monoclonal antibody directed against amyloid beta (Aβ), seemed promising for the development of disease-modifying strategies, such an approach requires further trials to verify its expected clinical benefits in AD. Therefore, there remains an urgent need for novel AD treatments.

Monoamine oxidase type B (MAO-B) is a flavin adenine dinucleotide (FAD)-containing enzyme located in the mitochondrial membrane of serotonin and histaminic neurons [1] and glial cells [2,3]. It catalyzes the oxidative deamination of neurotransmitters, such as dopamine [4,5], which is accompanied by the generation of reactive oxygen species causing toxicity to neuronal and glial cells [6].

The beneficial effects of MAO-B blockade in the early symptomatic treatment of Parkinson's disease have been well documented. MAO-B inhibitors may be used alone as monotherapy or as

* Corresponding author.
** Corresponding author.
E-mail addresses: katarzyna.grychowska@uj.edu.pl (K. Grychowska), pawel.zajdel@uj.edu.pl (P. Zajdel).

https://doi.org/10.1016/j.ejmech.2022.114329

add-on drugs (e.g., to levodopa). Nevertheless, these compounds gained interest as a potential approach to treating the cognitive decline associated with AD, considering the increased MAO-B levels in the brains of AD patients [7,8]. Indeed, the elevated level of MAO-B has been reported as an early event of AD which persists during the disease progression [9,10]. Additionally, an up-regulated MAO-B activity coincides with the presence of reactive astrocytes, during neuroinflammatory process in AD [11].

Clinical trials revealed that short-term treatment with selegiline, an irreversible MAO-B inhibitor, might reverse cognitive deficits in AD patients [12], whereas long-term administration of this drug had no significant effects [13]. Recent findings linking the activity of MAO-B and the expression of γ-aminobutyric acid (GABA) shed new light on the type of MAO-B inhibition and its potential impact on memory decline in AD. Pharmacological inhibition of MAO-B with irreversible inhibitors, which involves covalent modification of the active site of the enzyme, results in the destruction of the enzyme and the activation of alternative mechanisms to compensate for the level of GABA in reactive astrocytes [14]. On the other hand, reversible inhibitors (e.g., safinamide), which compete with the substrate at the binding site of MAO-B, do not damage the enzyme and thus do not induce unfavorable compensatory mechanisms [14].

In our recent studies on the series of 1*H*-pyrrolo[3,2-*c*]quinoline derivatives characterized by decreased basicity [15] and expected serotonin type 6 receptor (5-HT_6R) antagonistic properties [16–18], a new MAO-B inhibitor, compound **II**, was identified. This compound exhibited a decreased affinity for 5-HT_6R which resulted from the replacement of the basic nitrogen in the pyrrolidine fragment with an oxygen atom (**I**, **II** *vs* CPPQ, Fig. 1) [16]. The affinity for 5-HT_6R (**II** *vs* CPPQ) was further reduced when the N^1-sulfonyl moiety was replaced with a methylene bridge.

These results led to the search for MAO-B inhibitors among 1*H*-pyrrolo[3,2-*c*]quinolines and prompted us to investigate the structure–activity relationship of these compounds. In addition, we optimized the synthesis procedure for producing the PQ core using less toxic reagents. Structural modifications involved electron-donating and electron-withdrawing substituents at benzyl fragment, as well as alicyclic and aliphatic amines, aminoethers, and aminoalcohols at position 4, of the 1*H*-pyrrolo-[3,2-*c*] quinoline (PQ) core (Fig. 1).

Though some of the newly obtained derivatives inhibited MAO-B activity at a nanomolar or subnanomolar concentration, they exhibited high affinity for the human ether-à-go-go-related gene (*h*ERG) channel, which is responsible for the prolongation of the QT interval. Therefore, we performed off-target driven optimization to gain new structural insights into MAO-B inhibitors that do not exhibit affinity to *h*ERG channel. Furthermore, we assessed the pharmacokinetic properties of the most promising derivative and its glioprotective effect in cultured astrocytes exposed to cytotoxic doxorubicin (DOX). Finally, we carried out an *in vivo* evaluation of selected compounds to verify whether reversible MAO-B inhibitors derived from the PQ core could be promising compounds for the treatment of AD and exhibit procognitive properties and antidepressant-like activity.

2. Chemistry

The previously reported 1*H*-pyrrolo[3,2-*c*]quinoline core **7** [16] was synthesized using a procedure involving the aza-Baylis–Hillman reaction, *N*-allylation, and ring-closing metathesis (RCM) as the key steps. Although the optimized flow-chemistry approach used for RCM was fast and more environmentally friendly [19], the first two steps required the use of harmful reagents (methyl acrylate and allyl bromide) [16,17]. In order to replace this procedure with more sustainable methods, we applied the Leuckart-Wallach approach to convert commercially available 2-nitrobenzaldehyde **1** into respective formamide **2**, followed by the formation of isocyanide **3** after treatment with $POCl_3$ (Scheme 1) [20].

The resulting product **3** was subsequently heated with methyl propiolate in the presence of silver carbonate, which led to the formation of a nitro-derivative of methyl 2-phenyl-1*H*-pyrrole-3-carboxylate **4**. This allowed the synthesis of 2-aryl-1*H*-pyrrole carboxylate **4** in an overall yield of 30%, which is significantly higher than the yield of 21% obtained with the initial protocol (Table 1-SI) [21]. In addition, this approach enabled the synthesis of 2-aryl-1*H*-pyrrole-3-carboxylate **4** in three steps (one step less than previously), with the use of less toxic reagents compared to the RCM-based method (Scheme 1-SI) [21]. The subsequent steps proceeded following the reported synthetic routes. Reduction of the nitro group of **4** yielded aromatic amine derivative **5**, which was cyclized to lactam **6**, and then underwent a chlorodehydroxylation with $POCl_3$ to obtain 1*H*-pyrrolo[3,2-*c*]quinoline **7.** [16].

Heating of compound **7** with respective benzyl bromides in the presence of phosphazene base P1-*t*-Bu-tris(tetramethylene) (BTPP) yielded benzyl derivatives **8a**–**8h** (Scheme 2). Subsequent coupling with primary amines occurred under Buchwald–Hartwig *N*-arylation conditions, while reactions with secondary amines were carried out under prolonged microwave heating in acetonitrile in the presence of triethylamine (TEA).

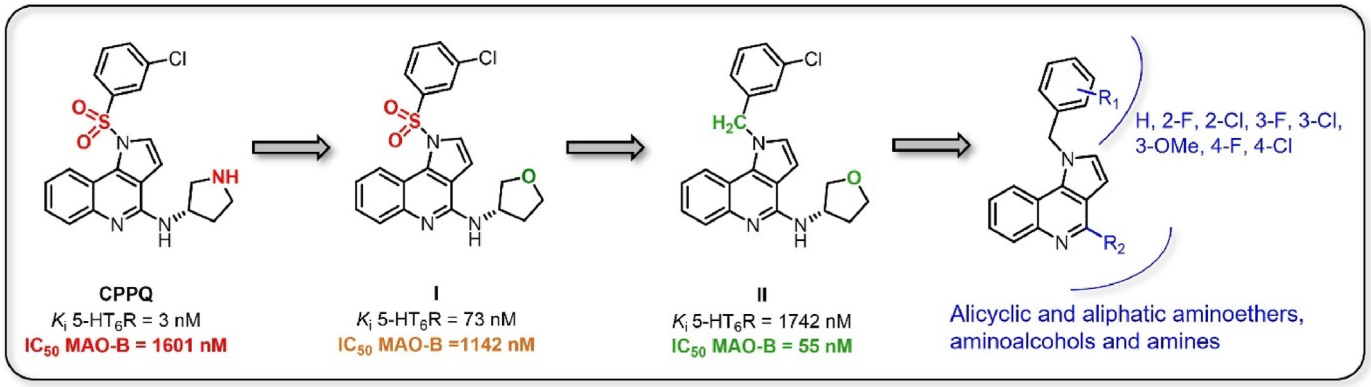

Fig. 1. Design strategy and structural modifications of novel 1*H*-pyrrolo-[3,2-*c*]quinoline derivatives.

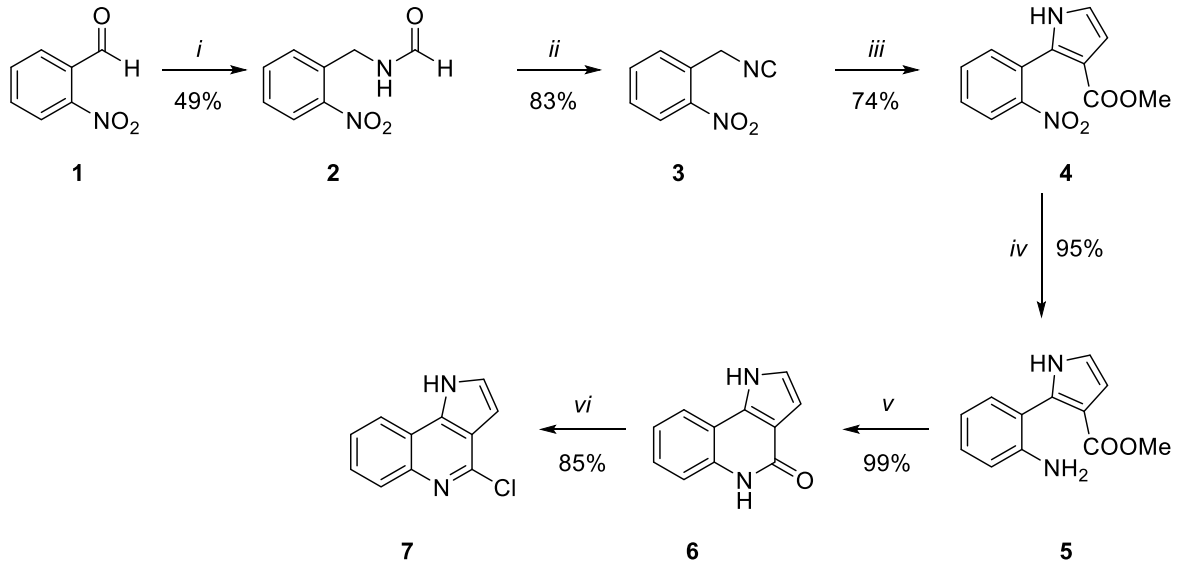

Scheme 1. Synthetic pathway leading to 1*H*-pyrrolo[3,2-*c*]quinoline **7**. (*i*) Formamide, HCOOH, CH_2Cl_2, 120 °C, 12 h; (*ii*) TEA, $POCl_3$, 0 °C, 30 min; (*iii*) Methyl propiolate, Ag_2CO_3, dioxane, 80 °C, 30 min; (*iv*) H_2, Pd/C, MeOH, rt, 2 h; (*v*) AcOH, *sec*-BuOH, 60 °C, 3 h; (*vi*) $POCl_3$, 105 °C, 4 h.

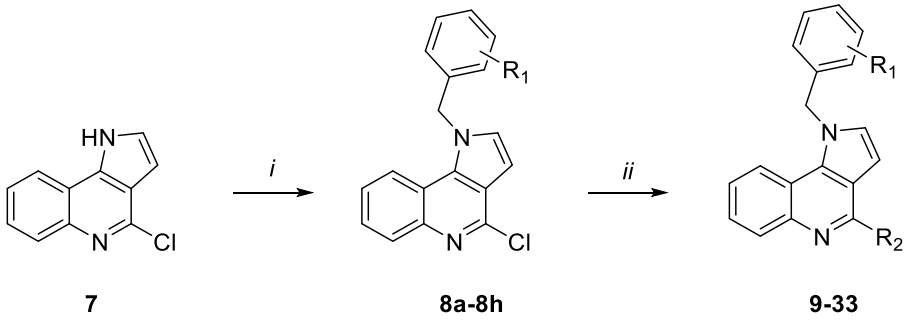

Scheme 2. Synthetic pathway leading to final compounds **9**–**33**. (*i*) BTPP, respective benzyl bromide, CH_2Cl_2, 36 C, 12 h *(ii)* Primary amine, *t*-BuONa, BINAP, $Pd_2(dba)_3$, dioxane/*t*-BuOH 3/1, 90 °C, 1 h, MW or secondary amine, acetonitrile, 140 °C, 7 h MW.

3. Results and discussion

3.1. Structure–activity relationship studies

Molecular docking studies of representative library derivatives were carried out on five MAO-B crystals structures containing a significant amount of water molecules (W1–W6; Fig. 1-SI and 2-SI). Surprisingly, no ligand–receptor complexes were identified in the analysis, which indicated that the conformational state of the enzyme, and thus the position of water molecules, may vary depending on the MAO-B crystals. Therefore, we performed a fully flexible docking procedure (induced fit-docking (IFD)), in which the conformational change occurred in the enzyme active site, FAD, inhibitor, and W1–W6 water molecules. Based on the best conformations determined in IFD, a series of dockings were performed for the selected compounds.

A comparative analysis of the binding modes of the initially identified analogs **I** and **II** (Fig. 2) revealed that the 2-aminotetrahydrofuranyl fragment was localized within the hydrophobic crevice formed by the FAD tricyclic system and Y398, Y326, and Y435 amino acid residues. The analysis showed a slight rotation of this group within both derivatives and the formation of a hydrogen bond with Y326. Six water molecules (W1–W6) were found to be conserved (Fig. 2-SI) and seem to support the orientation of noncovalent inhibitors within the active site of the enzyme (Fig. 2). Indeed, 1*H*-pyrrolo[3,2-*c*]quinoline fragment was

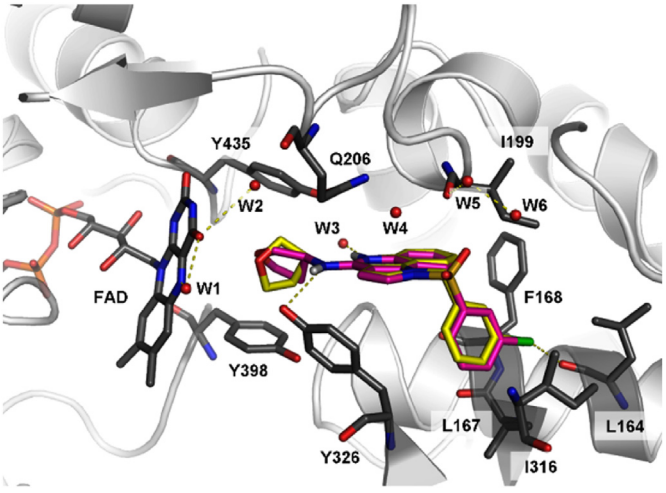

Fig. 2. Illustration of the binding mode of compounds **I** and **II** in the catalytic center of MAO-B enzyme obtained by the molecular docking: **I** (magenta) *vs* **II** (yellow).

positioned in the center of the catalytic pocket, forming a hydrogen bond with water molecule W3 and taking part in hydrophobic interactions with F168 and Y326. The 3-chlorobenzenesulfonyl and 3-chlorobenzyl fragments were located near the B entrance channel in both derivatives. The rotation of these fragments toward the channel was blocked by water molecules W5 and W6, which made them point toward the hydrophobic cavity formed by amino acids L167, I316, L164, and F168. In addition, the Cl substituent present at position 3 stabilized the orientation of the 3-chlorobenzyl fragment by forming a weak halogen bond with the carbonyl oxygen of L164. The 3-chlorobenzyl derivative **II** was characterized by higher inhibitory activity compared to its 3-chlorobenzenesulfonyl analog, which might be due to the limited rotation of the latter in the rigid binding pocket of MAO-B.

In vitro studies revealed that the newly synthesized compounds **9**–**33** had moderate-to-high inhibitory effect on MAO-B, with their IC_{50} values ranging from 0.7 to 289 nM, and no activity for MAO-A isoform (2–5% inhibition at 1 μM), as determined using the fluorometric method (Table 1).

The expansion of the tetrahydrofuranyl (THF) ring of compound **II** to the six-membered tetrahydropyranyl moiety contributed to maintaining its inhibitory activity on MAO-B and high selectivity over 5-HT_6R (**II** *vs* **9**). Further separation of the THF ring from the exocyclic amino group with the use of a methylene bridge revealed the importance of the distance between nitrogen and oxygen atoms in the aminoether fragment (**11** and **12**): attachment of the methylene spacer at C^2 position of THF caused a significant decrease in the MAO-B inhibitory activity (**11** *vs* **9**), while a shift of the spacer to

Table 1
Influence of the aminoether fragment on the MAO-B and MAO-A inhibitory activity, and affinity for 5-HT_6R and *h*ERG channel.

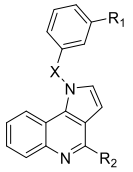

Compound	X	R_1	R_2	IC_{50} ± SEM [nM] MAO-B[a]	% inh MAO-A[b]	K_i ± SEM [nM] 5-HT_6R [c]	% inh *h*ERG[d]
I	-SO_2-	-Cl		1142	2	73	NT
II	-CH_2-	-Cl		55	4	1742	NT
9	-CH_2-	-Cl		3.4 ± 0	3	33060 ± 4567	NT
10	-CH_2-	-OMe		5 ± 0	2	3024 ± 275	72%
11	-CH_2-	-Cl	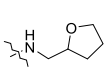	96 ± 2	3	696 ± 78	NT
12	-CH_2-	-Cl	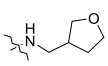	4.6 ± 0	4	838 ± 67	89%
13	-CH_2-	-H	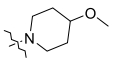	11 ± 2	3	NT	NT
14	-CH_2-	-Cl	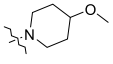	0.8 ± 0	2	799 ± 64	84%
15	-CH_2-	-OMe	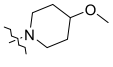	0.7 ± 0	5	740 ± 56	94%
16	-CH_2-	-Cl		16 ± 6	4	350 ± 27	NT
17	-CH_2-	-Cl	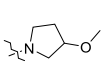	2.5 ± 0	2	NT	NT
	Rasagiline			15.4 ± 0.6	NT	NT	NT
	Safinamide			7 ± 1.2	NT	NT	NT

[a] IC_{50} values were determined by fluorometric method using human recombinant MAO-B and rasagiline [1 μM] as a positive control.
[b] % of inhibition of control (clorgyline, 1 μM) at 1 μM determined by fluorometric method using human recombinant MAO-A.
[c] Mean K_i values based on three independent binding experiments in HEK293 cells stably expressing *h*5-HT_6R.
[d] Performed in duplicate in dofetilide binding experiment at 1 μM using human recombinant *h*ERG.

Table 2
Influence of the spiroaminoether/aminoalcohol fragment on the MAO-B, and MAO-A inhibition activity, and affinity for 5-HT_6R and *h*ERG channel.

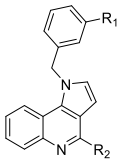

Compound	R_1	R_2	IC_{50} ± SEM [nM][a] MAO-B	% inh MAO-A[b]	K_i ± SEM [nM][c] 5-HT_6R	% inh *h*ERG[d]
18	-Cl		9.0 ± 0	2	2243 ± 246	**67**
19	-H		16 ± 6	6	992 ± 64	**76**
20	-Cl		42 ± 4	3	1362 ± 60	NT
21	-Cl	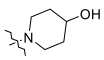	1.8 ± 0	4	1713 ± 121	**89**
22	-OMe	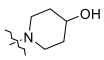	2.5 ± 0	7	1338 ± 68	NT
23	-Cl		11 ± 2	2	1227 ± 72	NT
24	-Cl	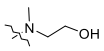	5.2 ± 1	3	40300 ± 3471	**68**

[a] IC_{50} values were determined by fluorometric method using human recombinant MAO-B and rasagiline [1 μM] as a positive control.
[b] % of inhibition of control (clorgyline, 1 μM) at 1 μM determined by fluorometric method using human recombinant MAO-A.
[c] Mean K_i values based on three independent binding experiments in HEK293 cells stably expressing *h*5-HT_6R.
[d] Performed in duplicate in dofetilide binding experiment at 1 μM using human recombinant *h*ERG.

Table 3
Influence of the amine fragment on the MAO-B, and MAO-A inhibition activity and affinity for *h*ERG channel.

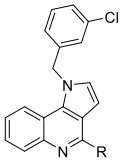

Compound	R	IC_{50} [nM][a] MAO-B	IC_{50} [nM][b] MAO-A	K_i ± SEM [nM][c] 5-HT_6R	% inh *h*ERG[d]
25		13 ± 1	NT	NT	77
26		9 ± 1	>100 μM	3827	42

[a] IC_{50} values were determined by fluorometric method using human recombinant MAO-B and rasagiline [1 μM] as a positive control.
[b] IC_{50} values and % of inhibition of control (clorgyline, 1 μM) at 1 μM determined by fluorometric method using human recombinant MAO-A.
[c] Mean K_i values based on three independent binding experiments in HEK293 cells stably expressing *h*5-HT_6R.
[d] Performed in duplicate in dofetilide binding experiment at 1 μM using human recombinant *h*ERG.

C^3 position was well-tolerated and did not affect the inhibitory potential (**12** *vs* **9**).

On the other hand, all aminoether derivatives **13**–**17**, containing an endocyclic nitrogen atom and an exocyclic oxygen atom, displayed potent MAO-B inhibitory effect. In particular, derivatives **14** and **15** bearing 4-methoxy piperidine showed inhibitory activity at subnanomolar concentrations.

Because several structurally and functionally unrelated central nervous system drugs can block the *h*ERG channel, a potassium channel responsible for the prolongation of QT interval in electrocardiogram, we evaluated the affinity of selected compounds for this channel (Table 1) [22]. We found that compounds **10**, **12**, **14**, and **15** showed a high affinity for *h*ERG at a concentration of 1 μM (72–94% inhibition of dofetilide binding at 1 μM) in the screening

procedure. Therefore, we included a screen for *h*ERG activity, as a key antitarget, in our lead-optimization workflow.

To reduce the affinity for the *h*ERG channel, we first replaced cyclic aminoether fragments with their spiro bioisosteres (i.e., 2-oxa-6-azaspiro[3.3]heptane and 2-oxa-6-azaspiro[3.4]octane) (Table 2). However, this modification had no impact on the affinity of compounds for *h*ERG (**18**, 67% inhibition). Moreover, changing the geometry of the aminoether fragment slightly decreased the MAO-B inhibitory activity (**18**, **20** *vs* **9**, **12**, **14**). Although subsequent replacement of the aminoethers with cyclic and aliphatic amino-alcohols, i.e., piperidine-4-ol, piperidine-3-ol, and 2-(methylamino) ethan-1-ol, allowed maintaining high MAO-B inhibitory activity (**21**–**24**), it did not significantly reduce the affinity of the compounds for *h*ERG (**21**, **24**).

We further hypothesized that activity at *h*ERG might be diminished by the removal of Lewis base oxygen atom. Nevertheless, the introduction of a piperidine moiety at position 4 of the pyrroloquinoline scaffold (**25**) did not cause a considerable decrease in the affinity for this antitarget (Table 3).

It is worth noting that the introduction of fluorine atoms in the structure of the molecule, which results in a decrease in the pK_a value, is one of the strategies applied for detuning the *h*ERG activity and improving metabolic stability of compounds [23]. Therefore, we introduced a *gem*-difluoro substituent at position 4 of piperidine fragment to obtain **26**. This modification allowed maintaining potent MAO-B inhibitory activity as well as safe *h*ERG affinity (**26** *vs* **25**). *In silico* docking studies confirmed that derivative **26** showed similarities to one of the most potent compounds from the series bearing 4-methoxypiperidine moiety (**14**; Fig. 3A) in terms of the location and type of interaction of the 4,4-difluoropiperidine fragment.

In parallel, the *in vitro* metabolic stability of compounds **25** and **26** was determined using the rat liver microsomes (RLM) assay. The results showed that compound **25** displayed a high intrinsic clearance (104 ml/min/kg), whereas its analog **26** showed lower clearance (29 ml/min/kg). This suggested that the *gem*-difluoro substituent had a positive effect on the biological properties of compounds.

Following the identification of 4,4-difluoropiperidin-1-yl as the optimal amine fragment, we further investigated the influence of the position of the substituent in the benzyl fragment on the MAO-B inhibitory activity (Table 4).

Using a computational protocol involving molecular dynamic simulations, *ab initio* docking (quantum polarized ligand docking, QPLD), and energy calculations applying the Molecular Mechanics Generalized Born Surface Area (MM-GBSA) method, we first estimated the energy gain of the halogenated derivatives at positions 2, 3, and 4 relative to the unsubstituted derivative **27**. The results showed that the derivatives substituted at position 3 gained the highest stabilization energy of the complex, whereas 2- and 4-substituted derivatives formed less stable complexes due to steric hindrance (Table 4). It was also found that the complex was additionally stabilized by the halogen bond formed between the 3-Cl substituent and the carbonyl oxygen of L164 (Fig. 3B).

In vitro studies revealed that the presence of substituent at position 3 favored the inhibitory activity (position 3 > position 2 > position 4). On the other hand, removal of the initially introduced chlorine atom (**27** *vs* **26**) as well as its replacement with fluorine (**30**) or electron-donating methoxy group (**31** *vs* **26**) was unfavorable. Thus, the applied modifications confirmed the importance of the chlorine atom at position 3 of the aromatic ring.

Table 4
Influence of a kind of substituent at the benzyl fragment on the MAO-B inhibitory activity.

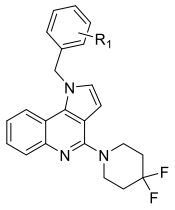

Compd	R_1	IC_{50} ± SEM [nM] MAO-B[a]	Average $\Delta\Delta G$[b]
26	3-Cl	9 ± 1	−12
27	H	89 ± 4	–
28	2-F	126 ± 15	−2
29	2-Cl	37 ± 4	−8
30	3-F	115 ± 15	0
31	3-OMe	45 ± 5	–
32	4-F	289 ± 44	0
33	4-Cl	201 ± 65	0

[a] IC_{50} values were determined by fluorometric method using human recombinant MAO-B and rasagiline [1 μM] as a positive control.
[b] The binding energy gain averaged by three complexes of each derivative selected from molecular dynamics simulations.

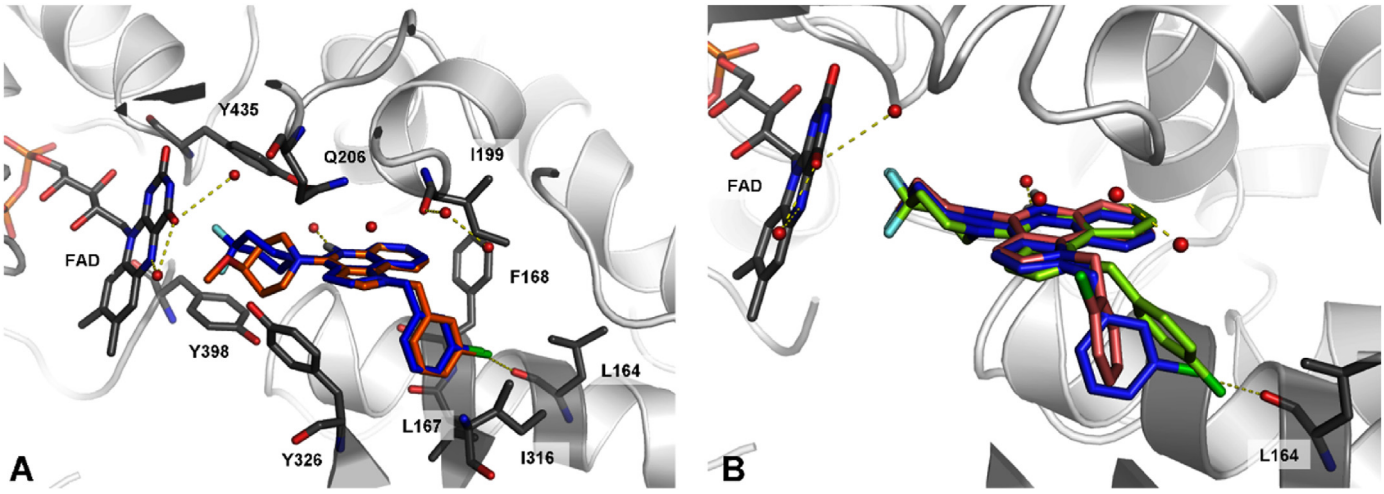

Fig. 3. Illustration of the binding mode of selected derivatives in the catalytic center of MAO-B enzyme obtained by the molecular docking: (**A**) **14** (orange), **26** (blue); (**B**) **29** (salmon) *vs* **26** (blue) *vs* **33** (lemon).

Table 5
Influence of a kind of substituent at the benzyl fragment on the metabolic stability of selected compounds.

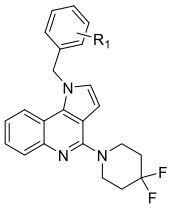

Compd	R_1	CL_{int} [ml/min/kg][a]
26	3-Cl	29
27	H	40
29	2-Cl	8
30	3-F	18
31	3-OMe	43

[a] Determined at a protein concentration of 0.4 mg/ml in RLM assay.

Selected compounds (IC_{50} < 120 nM) bearing the 4,4-difluoropiperidin-1-yl fragment displayed good metabolic stability in the RLM assay (Table 5).

3.2. Assessment of the MAO-B inhibitory activity of compound **26**

Kinetic studies using *in vitro* methods were performed to assess the inhibitory effect of compound **26** on MAO-B. In the first step, the reversibility of compound **26** was evaluated. Rasagiline and safinamide, which displayed irreversible and reversible MAO-B inhibitory activity, respectively, were used as references. To assess the inhibitor's activity tested compounds were preincubated with the enzyme and low concentration of the substrate for 30 min, followed by the 100-fold increase of substrate concentration. As can be seen on the plots obtained for rasagiline, an irreversible inhibitor, its preincubation with the enzyme resulted in the irreversible decrease of fluorescent product (resorufin) formation in MAO-B/Horseradish peroxidase (HRP)-coupled reaction (Fig. 4). In contrast, safinamide and **26** time-dependently increased MAO-B enzymatic activity, and thus behaved as reversible inhibitors (Fig. 4).

Compound **26** was then tested at three concentrations corresponding to its IC_{20}, IC_{50}, and IC_{80} values (4, 17, and 66 nM, respectively) to evaluate its reversible inhibition modality (Fig. 5). The results obtained from the kinetic experiment were used for constructing Michaelis–Menten curves related to the substrate concentration and determining the respective reaction rate (Fig. 5A). Transformation of the obtained data using the Lineweaver–Burk equation allowed generating a double-reciprocal plot (Fig. 5B). As could be seen on the Lineweaver–Burk plot, lines converge to the left of the y-axis and above the x-axis, which suggests a mixed mode of inhibition. Therefore, we assumed that compound **26** can bind unequally to the free enzyme and enzyme–substrate complex, displaying a higher affinity for the former. It should be noted that in our experimental conditions, safinamide, a reversible MAO-B inhibitor used as a reference, also displayed a mixed mode of inhibition (Fig. 5C and D).

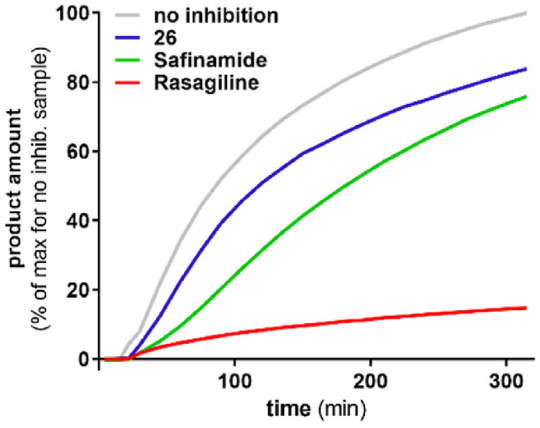

Fig. 4. Reactivation of MAO-B activity upon its blockade with **26** and reference inhibitors (safinamide and rasagiline) used at concentrations corresponding to their IC_{80} values in the presence of the substrate *p*-tyramine.

3.3. Selectivity profiling

Because early identification of the compound's affinity for off-targets might reduce safety-related attrition in further development, selectivity profiling was performed for compound **26**. We found that the lead compound showed significant selectivity for over 45 receptors (Table 6), enzymes, transporters, and ion channels (Table 7).

Interestingly, compound **26** displayed an affinity for sodium channels in the nonselective [^{3}H]-batrachotoxin binding (83.7% inhibition at 10 μM) (Table 7). Since blockade of sodium channels may cause inhibition of glutamate release from stimulated nerve terminals [24], this mechanism is regarded as a valid strategy of reducing overactive glutamate transmission. It may thus constitute an important added value to the MAO-B inhibitory activity of compound **26** [25]. Compound **26** did not inhibit the activity of sodium Nav1.5 channels (7.7% at 10 μM), which are one of the key anti-targets involved in the pathogenesis of cardiomyopathy (Table 7).

Moreover, compound **26** did not activate serotonin 5-HT_{2B}Rs (−15% at 10 μM) (Table 6), and the preliminary result from the dofetilide binding assay showed that it displayed weak interaction with *h*ERG channels (57% in electrophysiological QPatch experiment at 10 μM) (Table 7). This indicates that compound **26** does not induce cardiotoxic effects associated with these targets, such as valvulopathy and cardiac arrhythmia [26].

3.4. Preliminary safety profile assessment and evaluation of ADME/Tox properties

Modulation of cytochrome P450 (CYP450) can result in undesirable drug–drug interactions, which is an important safety concern in the drug development process. Because some MAO-B inhibitors have been recently reported to influence the activity of CYP450 [27], we evaluated compound **26** for its inhibitory effect on these enzymes. Compound **26** decreased the activity of CYP2C9 and CYP3A4 (21% and 59% respectively), but had no effect on CYP2D6 (92%).

Because drug-induced liver injury is one of the most serious concerns associated with drug withdrawal, compound **26** was subsequently tested in the human liver cancer cell line (HepG2) to assess its hepatotoxic effect. The MTS (3-(4,5-dimethylthiazol-2-yl)-5-(3-carboxymethoxyphenyl)-2-(4-sulfophenyl)-2*H*-tetrazolium inner salt) assay revealed that compound **26** did not affect the viability of the tested cells after exposure for 24 h (Fig. 3-SI). Additionally, the MTT (3-(4,5-dimethylthiazol-2-yl)-2,5-diphenyltetrazolium bromide) assay performed with an aim of assessing mitochondrial metabolism in C8-D1A astrocytes indicated that the compound **26** did not induce significant cytotoxicity at concentrations up to 5 μM. Finally, the AMES (*Salmonella typhimurium* reverse mutation) assay carried out for assessing mutations in the genes engaged in the histidine synthesis revealed that compound **26** did not show mutagenic effect at any tested concentration (1 or 10 μM) (Fig. 4-SI).

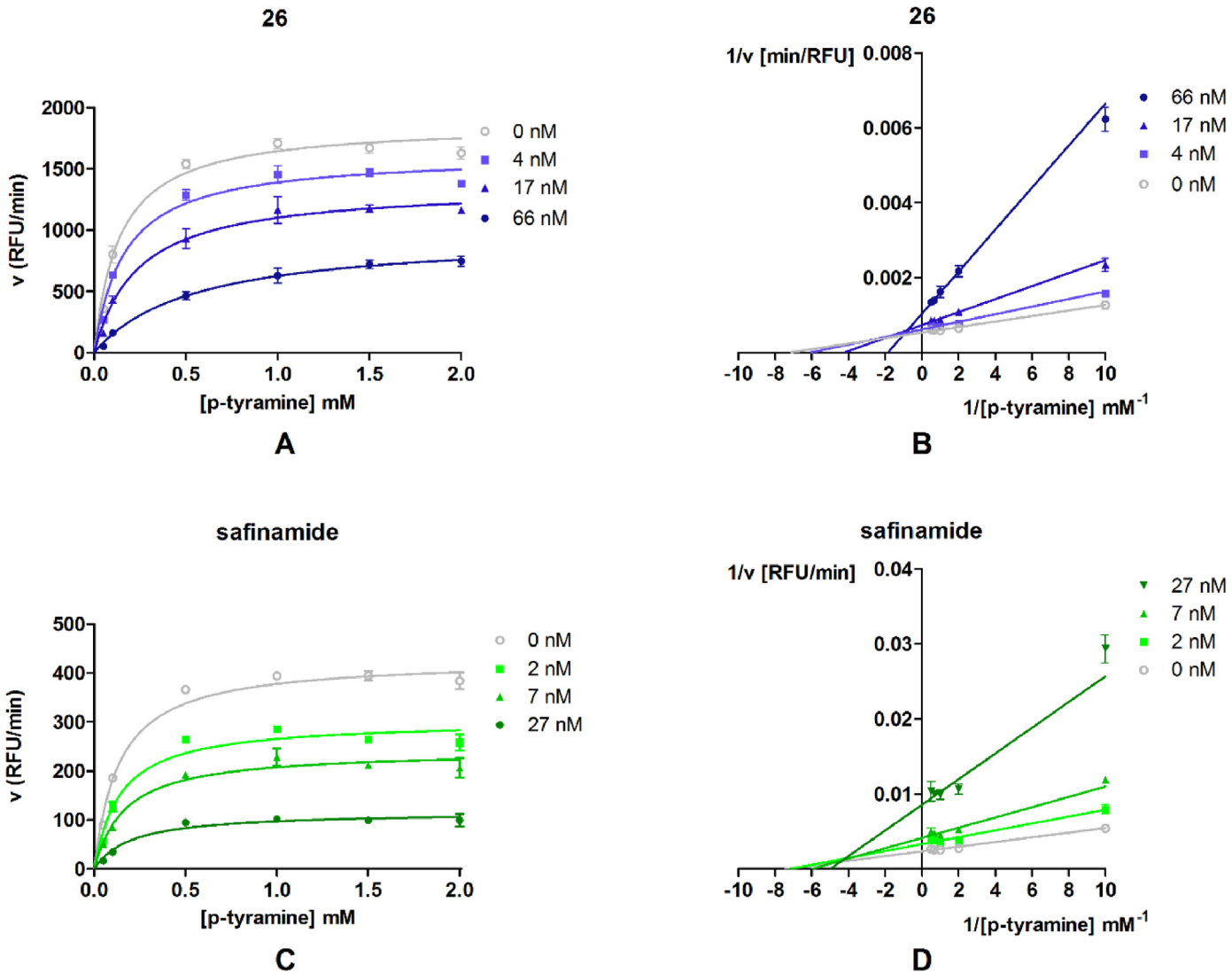

Fig. 5. Evaluation of modality of reversible inhibition of **26** and safinamide used as reference reversible inhibitor: Michaelis-Menten curves (A, C) and Lineweaver-Burk plots (B, D).

3.5. Glioprotective effects

Due to the uptake and degradation of Aβ, glial cells, particularly astrocytes, have been shown to play a protective role in the early stage of AD. However, as the disease progresses, the astrocyte clearance of this protein/peptide decreases [28]. The resulting accumulation of Aβ stimulates astrocytes to produce pro-inflammatory agents [29].

We examined the glioprotective effects of compound **26** in a model of cultured astrocytes (C8-D1A), exposed to DOX, a cytotoxic agent. DOX-induced cell death occurs as a result of alterations in synaptic plasticity, apoptosis, and lipid peroxidation. The MTT assay showed that compound **26** protected C8-D1A astrocytes at 0.25 μM against DOX-induced cytotoxicity (Fig. 6). On the other hand, neither selegiline nor safinamide used as a reference compounds displayed a significant glioprotective effect.

3.6. Pharmacokinetics evaluation

To investigate the preliminary pharmacokinetic profile of compound **26**, we determined its concentrations in plasma (Fig. 7a) and brain (Fig. 7b) in Sprague Dawley rats at various time points following oral and intravenous administration (3 mg/kg).

A direct comparison of the area-under-the-curve values determined after both oral and intravenous administration indicated that compound **26** displayed excellent bioavailability of 94.9%. Further analysis of brain tissue showed that it crossed the blood–brain barrier and reached maximal concentration (C_{max}) of 110.7 ng/ml after 2 h of oral administration. Its brain-to-plasma concentration ratio after intravenous and intragastric administration was 1.03 and 1.43, respectively. Compound **26** was eliminated from the body with a half-life of 148 and 188 min after intravenous and intragastric administration, respectively.

3.7. Effects on scopolamine-induced cognitive deficit

As cognitive impairment in AD is accompanied by decreased cholinergic neurotransmission, we assessed the potential procognitive effects of compound **26** in rats treated with anticholinergic scopolamine to induce cognitive deficits in the novel object recognition (NOR) test [30]. The results showed that compound **26** administered orally 2 h before the acquisition trial prevented scopolamine-induced short-term memory deficits ($F(3,35) = 15.7$, $p < 0.0001$; Fig. 8).

Table 6
Cellular and nuclear receptor functional assays of 26[a].

Target	Agonist effect	Antagonist effect
A_{2A}	−0.3	−31.2
α_{1A}	0.5	13.2
α_{2A}	6.3	7.5
β_1	0.7	−8.6
β_2	−0.3	−14.5
CB_1	53.4	11.3
CB_2	−12.5	14.2
CCK_1	0.5	20.9
D_1	−1.4	−14.6
D_{2L}	−0.8	−3.9
ET_A	1.9	−20.7
H_1	2.5	−1.3
H_2	−0.1	12.8
κ (KOP)	−1.7	0.8
M_1	0.7	3.8
M_2	20.7	4.1
M_3	0.7	4.9
δ (DOP)	−3.0	14.8
μ (MOP)	−19.9	3.4
5-HT_{1A}	−0.3	−1.0
5-HT_{1B}	−0.6	0.6
5-HT_{2A}	1.5	4.7
5-HT_{2B}	−15.0	14.5
V_{1A}	−3.0	−15.3

[a] Performed at Eurofins. Testing concentration 10 μM.

Table 7
Selectivity profiling of 26 over selected molecular targets. [a]

Target	% Inhibition	Target	% Inhibition
σ_1	71.5[b]	NET	18.0[c]
σ_2	73.5[b]	DAT	46.3[c]
5-HT_3	5.4 [b]	SERT	18.1[c]
Ca^{2+} channel (N)	−1.4[b]	*h*Cav3.2	1.1[d]
Na^+ channel (site 2)	83.7[b]	*h*Cav1.2	19.8[d]
COX1	17.2[c]	*h*Nav1.5	7.7[d]
COX2	22.2[c]	*h*ERG	57.7[d]
PDE3A	36.2[c]	hKCNQ1/minK	19.1[d]
PDE4D2	41.7[c]	*h*nAChR α4/β2	6.44[e]
Lck kinase	4.0[c]	*h*GABAA α1/β2/γ2	101.2[e]
AChE	−6.7[c]		

[a] Performed at Eurofins. Testing concentration 10 μM.
[b] Binding assays.
[c] Enzyme and uptake assays.
[d] Electrophysiological QPatch assay.
[e] Ion flux assay.

3.8. Antidepressant properties

Since depression is a common comorbid condition in AD, we finally assessed the potential antidepressant-like activity of compound **26** in mice by performing forced swim test (FST). Of note, selegiline produced antidepressant-like activity in the *in vivo* preclinical models [31,32], and showed significant antidepressant effect in treatment-resistant depression [33]. Additionally, clinical trials confirmed efficacy of safinamide in treating depressive symptoms [34–36] and improving of the mood [35] in Parkinson's disease (PD) patients. Likewise, concomitant use of safinamide with antidepressant drugs (e.g., selective serotonin reuptake inhibitors) in PD patients was well-tolerated and such treatment did not evoke serotonin syndrome [36].

The results revealed that the compound (0.312–2.5 mg/kg) exhibited antidepressant-like properties, at one dose of 0.625 mg/kg shortening the immobility time by 36.5% (Fig. 9). Of note, the potency of **26** administered at a dose of 0.625 mg/kg was similar to that of the antidepressant drug *S*-citalopram achieved with a two-time higher dose (1.25 mg/kg). Compound **26** showed a U-shaped dose–response curve, whereas *S*-citalopram dose-dependently shortened immobility time.

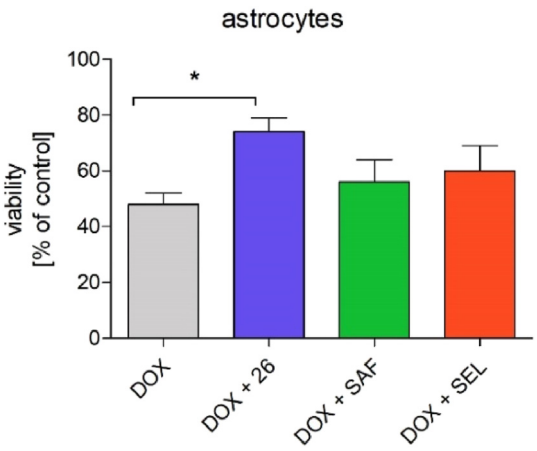

Fig. 6. Effects of **26**, safinamide and selegiline on doxorubicine-induced astrocytes cytotoxicity. MTT assay was performed on astrocytes co-treated with tested compounds (0.25 μM) and DOX (0.5 μM) for 24 h period. Data are expressed as mean ± SEM. Statistical significance (*) was calculated relative to DOX ($p < 0.05$).

Active doses of the investigated compound **26** and the reference drug had no effect on the spontaneous locomotor activity measured over the observation period in the FST (i.e., from 2 to 6 min). This suggests that the antidepressant effects of these compounds are specific (data not shown).

4. Conclusions

Because of the well-known effects of fluorine on the physicochemical properties and biological activity of compounds, this element has been widely incorporated in chemical structures in the drug optimization process. In this study, we performed a systematic structure–activity relationship analysis and identified compound **26** (1-(3-chlorobenzyl)-4-(4,4-difluoropiperidin-1-yl)-1*H*-pyrrolo[3,2-*c*]quinoline), a potent reversible MAO-B inhibitor. Most importantly, this compound was obtained using less toxic agents, by applying a new protocol for the synthesis of pyrroloquinoline core. The obtained compound **26** displayed a low affinity for the *h*ERG channel as well as good metabolic stability, which could be attributed to the introduction of fluorine atoms. Moreover, the compound showed selectivity for over 45 targets, a favorable safety profile, and brain permeability. The derivative **26** also demonstrated glioprotective effects against DOX in a model of cultured astrocytes. In *in vivo* evaluation, compound **26** reversed scopolamine-induced cognitive deficits in the NOR test in rats and displayed antidepressant-like activity in FST in mice. Taken together, these results suggest that fluorination strategy can be successfully applied in medicinal chemistry for the development of selective MAO-B inhibitors devoid of *h*ERG channel activity.

5. Experimental

5.1. Chemistry

5.1.1. General methods

The synthesis was conducted at room temperature, unless indicated otherwise. Organic solvents (from Sigma-Aldrich and Chempur) were of reagent grade and were used without purification. All reagents (Sigma-Aldrich, Fluorochem and TCI) were of the highest purity.

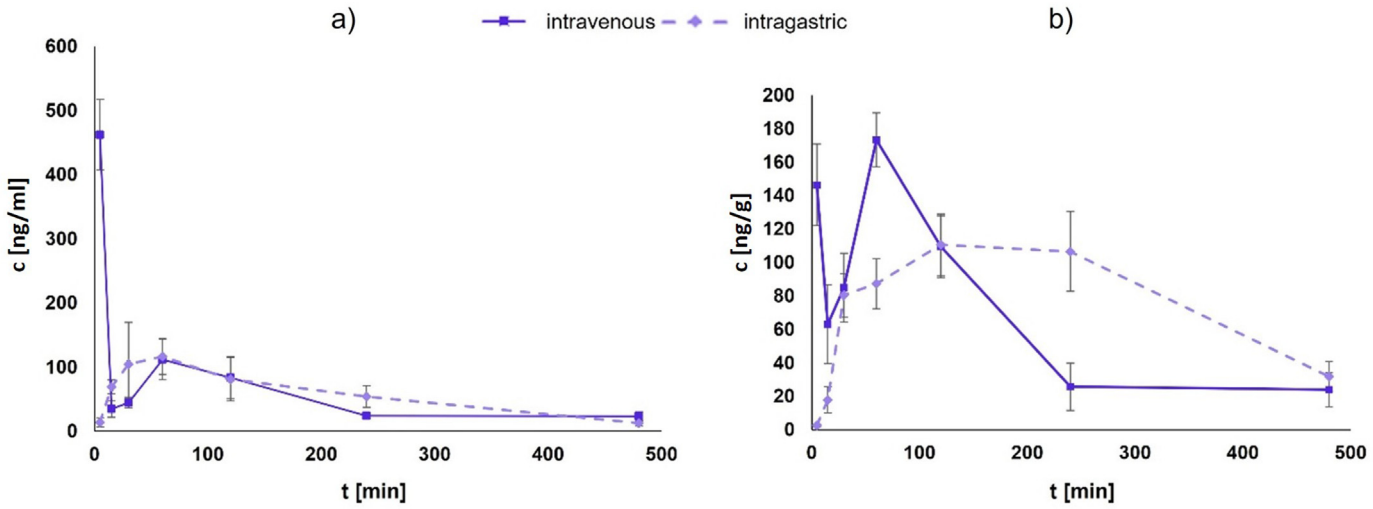

Fig. 7. Time dependence of plasma (a) and brain (b) concentration in the rat after a single intravenous and intragastric administration of compound **26** at 3 mg/kg (linear scale).

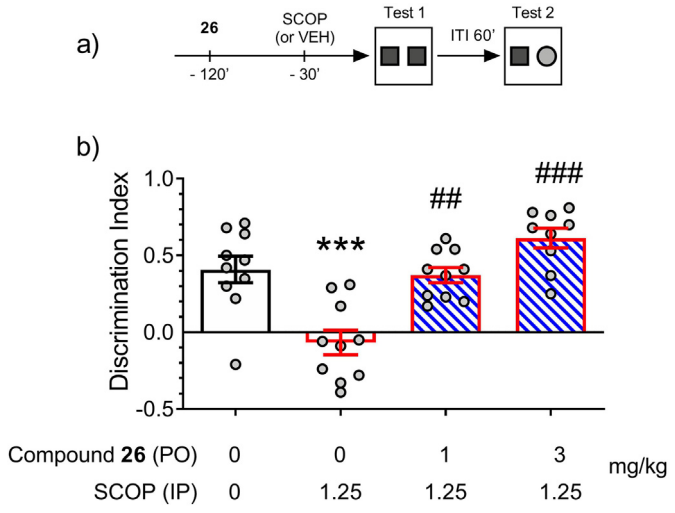

Fig. 8. a) Novel Object Recognition test experimental design, b) Effects of compound **26** (1 and 3 mg/kg, PO) on scopolamine (1.25 mg/kg, *i.p.*)-induced cognitive deficits in the NOR task in rats suggest that **26** prevents learning impairment and displays decent *in vivo* effects following oral administration. Compound **26** was administered 90 min before scopolamine, which was administered 30 min before the familiarization trial (T1). Novel object recognition was investigated at the recognition trial (T2), 60 min later. Data are expressed as the mean ± SEM of the Discrimination Index and drug doses, expressed as mg/kg, are shown in the legend below the abscissa. N = 9–10 rats per treatment. Symbols: VEH, vehicle; ***p < 0.001 *vs* control (VEH/VEH), ##p < 0.01; ###p < 0.001 *vs* VEH/scopolamine, Newman-Keuls multiple comparison post-hoc test.

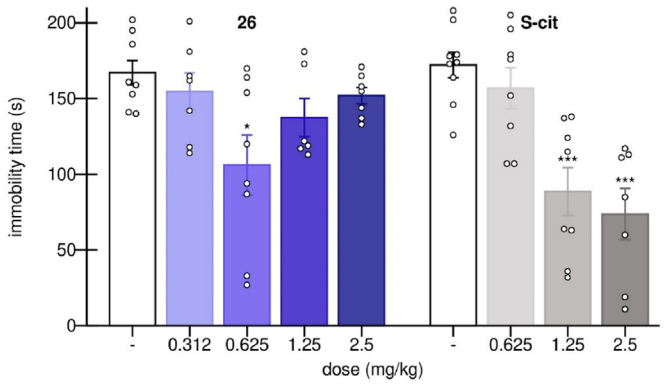

Fig. 9. Effect of compound **26** and *S*-citalopram on immobility time in mice in the forced swim test after intraperitoneal (*i.p.*) administration 60 min before the test. Data are presented as the mean ± standard error of the mean of N = 7–9 animals per group. *p < 0.05 compared with the vehicle group, followed by Bonferroni's comparison test after significant analysis of variance; F(4,31) = 3.4901, p = 0.018.

Column chromatography was performed on silica gel Merck 60 (70–230 mesh ASTM).

UPLC and MS were carried out on a system consisting of a Waters Acquity UPLC coupled to a Waters TQD mass spectrometer. All the analyses were carried out using an Acquity UPLC BEH C18 100 × 2.1 mm^2 column at 40 °C. A flow rate of 0.3 ml/min and a gradient of (0–100)% B over 10 min was used: eluent A, water/0.1% HCOOH; eluent B, acetonitrile/0.1% HCOOH. Retention times, t_R, were given in minutes. The UPLC/MS purity of all the test compounds and key intermediates was determined to be >95%.

High-resolution MS measurements were performed on a Bruker Impact II mass spectrometer (Bruker Corporation, Billerica, USA). Electrospray ionization (ESI) was used in the positive ion mode. Mass accuracy was within 2 ppm error in full-scan mode. The optimized MS parameters were the following: ion spray voltage 4 kV; capillary temperaturę 240 °C, dry gas flow rate 4 l/min. High-purity nitrogen as the nebulizing gas was used. Samples of 50 μM concentration were prepared from tested compounds using an eluent of acetonitrile/water 80:20 (v/v)/1% HCOOH.

^{1}H NMR and ^{13}C NMR spectra were recorded using JEOL JNM-ECZR 500 RS1 (ECZR version) at 500 and 126 MHz, respectively and are reported in ppm using deuterated solvent for calibration ($CDCl_3$, methanol-d_4 or dmso-d_6). The *J* values are given in Hertz (Hz). Melting points were determined with Buchi apparatus and are uncorrected.

Compounds **5**–**7** were obtained according to the previously reported procedure and the analytical data are in accordance with the literature [16]. Compound **26** selected for behavioral evaluation was converted into the hydrochloride salt.

*5.1.1.1. N-(2-nitrobenzyl)formamide (**2**).* Nitrobenzaldehyde **1** (35 g, 1 eq) was dissolved in HCOOH (70 ml, 8 eq) and formamide (110 ml, 12 eq) was added. The mixture was stirred at 120 °C for 16 h. Subsequently, the solution was diluted with CH_2Cl_2 and washed three times with water and saturated solution of NaCl. The organic phase was dried over Na_2SO_4, filtered and evaporated under reduced pressure. The residue was added AcOEt to precipitate a

yellow solid, which was filtered and dried under vacuum.

Yellow solid, yield 49%, t_R = 3.28 min, Mp 86–88 °C, $C_8H_8N_2O_3$, MW 180.16. ^{1}H NMR (500 MHz, $CDCl_3$) δ ppm 4.71 (d, J = 6.6 Hz, 2H), 6.25–6.61 (m, 1H), 7.48 (s, 1H), 7.58–7.65 (m, 1H), 7.65–7.70 (m, 1H), 8.07 (dd, J = 8.02, 1.2 Hz, 1H), 8.23 (s, 1H). Monoisotopic mass 180.05, $[M+H]^+$ = 181.3.

*5.1.1.2. 1-(Isocyanomethyl)-2-nitrobenzene (**3**).* Compound **2** (20 g, 1 eq) was dissolved in 300 ml of CH_2Cl_2 followed by addition of TEA (77 ml, 5 eq) and $POCl_3$ (10 ml, 1 eq). The mixture was stirred at 0 °C for 30 min. The solution was then diluted with CH_2Cl_2 and washed with saturated solution of $NaHCO_3$ and NaCl. The organic phase was dried over Na_2SO_4, filtered and evaporated under reduced pressure. The crude product was purified by chromatography on silica gel using CH_2Cl_2 as developing solvent.

Yellow solid, yield 83%, t_R = 3.31 min, Mp 147–149 °C, $C_8H_6N_2O_2$, MW 162.15. ^{1}H NMR (500 MHz, $CDCl_3$) δ ppm 5.16 (s, 2H), 7.54–7.62 (m, 1H), 7.78 (m, 1H), 7.77–7.90 (dd, J = 7.9, 1.0 Hz, 1H), 8.22 (dd, J = 8.2, 1.3 Hz, 1H).

*5.1.1.3. Methyl 2-(2-nitrophenyl)-1H-pyrrole-3-carboxylate (**4**).* Methyl propiolate (4 ml, 1.5 eq) and Ag_2CO_3 (0.8 g, 0.1 eq) were suspended in dioxane and compound **3** (4.8 g, 1 eq) dissolved in dioxane was added dropwise into the reaction mixture. The mixture was stirred at 80 °C for 30 min. Subsequently, the solution was filtered and the filtrate was evaporated under reduced pressure. The crude product was purified by chromatography on silica gel using AcOEt/Hex 4/6 as a developing solvent.

Yellow oil, 74% yield, t_R = 5.12 min, $C_{12}H_{10}N_2O_4$, MW 246.22. ^{1}H NMR (500 MHz, $CDCl_3$) δ ppm 3.61 (s, 3H), 6.67–6.73 (m, 1H), 6.79–6.85 (m, 1H), 7.44–7.47 (m, 1H), 7.50–7.56 (m, 1H), 7.58–7.64 (m, 1H), 7.99–8.03 (m, 1H), 8.58–8.69 (m, 1H). Monoisotopic mass 246.06, $[M+H]^+$ = 247.3.

*5.1.2. General procedure for preparation of compounds **8a**–**8h***

Compound **7** (0.28 mmol, 1 eq) was dissolved in CH_2Cl_2 (5 ml), and BTPP (170 μL, 0.56 mmol, 2 eq) was added, followed by addition of respective benzyl chloride (1.8 eq). The reaction mixture was stirred for 12 h. Subsequently, the mixture was evaporated, and the remaining crude product was purified by chromatography on silica gel using AcOEt/Hex as a developing solvent.

*5.1.2.1. 1-Benzyl-4-chloro-1H-pyrrolo[3,2-c]quinoline (**8a**).* White solid, yield 92%, t_R = 7.73 min, Mp 122–123 °C, $C_{18}H_{13}ClN_2$, MW 292.76. ^{1}H NMR (500 MHz, $CDCl_3$) δ ppm 5.80 (s, 2H), 6.87–6.92 (m, 1H), 7.03–7.09 (m, 2H), 7.20 (d, J = 3.1 Hz, 1H), 7.27–7.35 (m, 3H), 7.36–7.41 (m, 1H), 7.50–7.58 (m, 1H), 7.96–8.02 (m, 1H), 8.08–8.15 (m, 1H). Monoisotopic mass 292.08, $[M+H]^+$ = 293.0.

*5.1.2.2. 4-Chloro-1-(2-fluorobenzyl)-1H-pyrrolo[3,2-c]quinoline (**8b**).* White solid, yield 85%, t_R = 7.79 min, Mp 143–145 °C, $C_{18}H_{12}ClFN_2$, MW 310.76. ^{1}H NMR (500 MHz, $CDCl_3$) δ ppm 5.82 (s, 2H), 6.55–6.70 (m, 1H), 6.85–7.01 (m, 2H), 7.11–7.23 (m, 2H), 7.24–7.33 (m, 1H), 7.37–7.48 (m, 1H), 7.51–7.63 (m, 1H), 7.88–7.97 (m, 1H), 8.10–8.15 (m, 1H). Monoisotopic mass 310.07, $[M+H]^+$ = 311.2.

*5.1.2.3. 4-Chloro-1-(2-chlorobenzyl)-1H-pyrrolo[3,2-c]quinoline (**8c**).* White solid, yield 80%, t_R = 7.81 min, Mp 148–150 °C, $C_{18}H_{12}Cl_2N_2$, MW 327.21. ^{1}H NMR (500 MHz, $CDCl_3$) δ ppm 5.80 (s, 2H), 6.40 (d, J = 7.7 Hz, 1H), 6.91 (d, J = 2.8 Hz, 1H), 7.03 (s, 1H), 7.13–7.27 (m, 2H), 7.35–7.43 (m, 1H), 7.45–7.59 (m, 2H), 7.72–7.80 (m, 1H), 8.10–8.14 (m, 1H). Monoisotopic mass 326.04, $[M+H]^+$ = 327.0.

*5.1.2.4. 4-Chloro-1-(3-fluorobenzyl)-1H-pyrrolo[3,2-c]quinoline (**8d**).* White solid, yield 85%, t_R = 7.77 min, Mp 147–149 °C, $C_{18}H_{12}ClFN_2$, MW 310.76. ^{1}H NMR (500 MHz, $CDCl_3$) δ ppm 5.78 (s, 2H), 6.73 (d, J = 9.2 Hz, 1H), 6.82 (d, J = 8.0 Hz, 1H), 6.90 (d, J = 3.4 Hz, 1H), 6.94–7.00 (m, 1H), 7.20 (d, J = 2.9 Hz, 1H), 7.26–7.32 (m, 1H), 7.37–7.42 (m, 1H), 7.53–7.58 (m, 1H), 7.88–7.94 (m, 1H), 8.08–8.15 (m, 1H). Monoisotopic mass 310.07, $[M+H]^+$ = 311.2.

*5.1.2.5. 4-Chloro-1-(3-chlorobenzyl)-1H-pyrrolo[3,2-c]quinoline (**8e**).* White solid, yield 80%, t_R = 7.79 min, Mp 148–150 °C $C_{18}H_{12}Cl_2N_2$, MW 327.21. ^{1}H NMR (500 MHz, $CDCl_3$) δ ppm 5.77 (s, 2H) 6.84–6.94 (m, 2H) 7.05–7.10 (m, 2H) 7.17–7.24 (m, 2H) 7.41 (m, 1H) 7.50–7.57 (m, 1H) 7.88–7.96 (m, 1H) 8.09–8.16 (m, 1H). Monoisotopic mass 326.04, $[M+H]^+$ = 327.0.

*5.1.2.6. 4-Chloro-1-(3-methoxybenzyl)-1H-pyrrolo[3,2-c]quinoline (**8f**).* White solid, yield 95%, t_R = 7.66 min, Mp 184–186 °C, $C_{19}H_{15}ClN_2O$, MW 322.79. ^{1}H NMR (500 MHz, $CDCl_3$) δ ppm 3.69 (s, 3H), 5.76 (s, 2H), 6.55–6.68 (m, 2H), 6.81 (dd, J = 8.1, 2.2 Hz, 1H), 6.89 (d, J = 3.1 Hz, 1H), 7.18–7.25 (m, 2H), 7.35–7.42 (m, 1H), 7.49–7.57 (m, 1H), 8.00 (dd, J = 8.5, 1.0 Hz, 1H), 8.08–8.14 (m, 1H). Monoisotopic mass 322.09, $[M+H]^+$ = 323.1.

*5.1.2.7. 4-Chloro-1-(4-fluorobenzyl)-1H-pyrrolo[3,2-c]quinoline (**8g**).* White solid, yield 85%, t_R = 7.77 min, Mp 140–141 °C, $C_{18}H_{12}ClFN_2$, MW 310.76. ^{1}H NMR (500 MHz, $CDCl_3$) δ ppm 5.78 (s, 2H), 6.57–6.71 (m, 2H), 6.95 (d, J = 3.4 Hz, 1H), 6.98–7.08 (m, 1H), 7.22 (d, J = 2.9 Hz, 1H), 7.28–7.37 (m, 1H), 7.39–7.44 (m, 1H), 7.75–7.83 (m, 1H), 7.88–7.94 (m, 1H), 8.08–8.14 (m, 1H). Monoisotopic mass 310.07, $[M+H]^+$ = 311.2.

*5.1.2.8. 4-Chloro-1-(4-chlorobenzyl)-1H-pyrrolo[3,2-c]quinoline (**8h**).* White solid, yield 80%, t_R = 7.80 min, Mp 148–150 °C, $C_{18}H_{12}Cl_2N_2$, MW 327.21. ^{1}H NMR (500 MHz, $CDCl_3$) δ ppm 5.79 (s, 2H) 6.86–6.93 (m, 2H) 7.10–7.15 (m, 2H) 7.19–7.22 (m, 2H) 7.38 (m, 1H) 7.72–7.80 (m, 1H) 7.88–7.96 (m, 1H) 8.09–8.16 (m, 1H). Monoisotopic mass 326.04, $[M+H]^+$ = 327.0.

*5.1.3. General procedure for preparation of compounds **9**–**12** and **24***

Compound **8** (0.3 mmol, 1 eq) was mixed together with $Pd_2(dba)_3$ (0.02 eq), BINAP (0.04 eq), and NaO*t*-Bu (1.4 eq). The solids were suspended in 4 ml of a mixture of dioxane and *tert*-butanol (3/1, v/v), and respective amine (1.2 eq) was added. The reaction was irradiated with microwaves at 120 °C for 1 h under argon atmosphere. The resulting mixture was filtrated through a pad of Celite, concentrated and purified by column chromatography on silica gel using CH_2Cl_2/MeOH as a developing solvent.

*5.1.3.1. 1-(3-Chlorobenzyl)-N-(tetrahydro-2H-pyran-4-yl)-1H-pyrrolo[3,2-c]quinolin-4-amine (**9**).* White solid, yield 83%, t_R = 1.47 min, Mp 206–207 °C, $C_{23}H_{22}ClN_3O$, MW 391.89. ^{1}H NMR (500 MHz, methanol-d_4) δ ppm 1.32–1.47 (m, 2H), 1.80–1.92 (m, 2H), 3.35–3.44 (m, 2H), 3.67–3.82 (m, 2H), 4.25–4.38 (m, 1H), 5.39 (s, 2H), 6.45–6.56 (m, 1H), 6.60 (t, J = 4.2 Hz, 1H), 6.72 (s, 1H), 6.77–6.86 (m, 2H), 6.92 (dd, J = 5.0, 3.1 Hz, 2H), 7.09 (td, J = 7.8, 2.9 Hz, 1H), 7.41 (dd, J = 8.1, 3.2 Hz, 1H), 7.67 (s, 1H). ^{13}C NMR (126 MHz, $CDCl_3$) δ ppm 33.37, 52.75, 67.02, 112.0, 112.72, 118.18, 120.35, 128.20, 130.49, 159.96. Monoisotopic mass 391.15, $[M+H]^+$ = 392.1. HRMS (ESI): *m/z* calculated for $[M+H]^+$ 392.1529, found 392.1528.

*5.1.3.2. 1-(3-Methoxybenzyl)-N-(tetrahydro-2H-pyran-4-yl)-1H-pyrrolo[3,2-c]quinolin-4-amine (**10**).* White solid, yield 66%, t_R = 1.39 min, Mp 138–139 °C, $C_{24}H_{25}N_3O_2$, MW 387.47. ^{1}H NMR

(500 MHz, $CDCl_3$/methanol-d_4) δ ppm 1.69 (d, J = 6.1 Hz, 2H), 2.22 (ddd, J = 12.6, 4.6, 2.2 Hz, 2H), 3.66 (td, J = 11.6, 2.2 Hz, 2H), 3.71 (s, 3H), 4.06 (dt, J = 11.7, 3.6 Hz, 2H), 4.59 (s, 1H), 5.70 (s, 2H), 6.59 (dd, J = 2.5, 1.6 Hz, 1H), 6.65 (ddd, J = 7.6, 1.7, 0.9 Hz, 2H), 6.80 (dd, J = 8.2, 2.6 Hz, 1H), 7.05–7.15 (m, 2H), 7.23 (t, J = 7.9 Hz, 1H), 7.40 (t, J = 7.8 Hz, 1H), 7.81 (dd, J = 8.2, 1.3 Hz, 1H), 7.85 (s, 1H). ^{13}C NMR (126 MHz, $CDCl_3$) δ ppm 33.65, 53.14, 55.08, 66.84, 111.97, 112.67, 118.13, 120.38, 130.12, 160.10. Monoisotopic mass 387.19, $[M+H]^+$ = 388.2. HRMS (ESI): *m/z* calculated for $[M+H]^+$ 388.2025, found 388.2027.

*5.1.3.3. 1-(3-Chlorobenzyl)-N-((tetrahydrofuran-2-yl)methyl)-1H-pyrrolo[3,2-c]quinolin-4-amine (**11**).* White solid, yield 40%, t_R = 5.48 min, Mp 185–187 °C, $C_{23}H_{22}ClN_3O$, MW 391.90. ^{1}H NMR (500 MHz, $CDCl_3$/methanol-d_4) δ ppm 1.72–1.85 (m, 1H), 1.91–2.03 (m, 2H), 2.07–2.19 (m, 1H), 3.71 (d, J = 6.5 Hz, 1H), 3.81–3.90 (m, 1H), 3.93–4.02 (m, 1H), 4.10 (d, J = 13.5 Hz, 1H), 4.25–4.28 (m, 1H), 5.69 (s, 2H), 6.95 (dt, J = 7.3, 1.6 Hz, 1H), 6.98 (d, J = 3.2 Hz, 1H), 7.03–7.08 (m, 2H), 7.16 (td, J = 8.4, 7.0, 1.4 Hz, 1H), 7.21–7.25 (m, 2H), 7.40 (ddd, J = 8.4, 7.0, 1.4 Hz, 1H), 7.73 (dd, J = 8.2, 1.2 Hz, 1H), 7.82 (dd, J = 8.3, 1.4 Hz, 1H). ^{13}C NMR (126 MHz, $CDCl_3$/methanol-d_4) δ ppm 26.10, 28.94, 52.85, 68.45, 78.66, 120.50, 124.17, 126.16, 128.29, 130.58, 135.27. Monoisotopic mass 391.15, $[M+H]^+$ = 392.4. HRMS (ESI): *m/z* calculated for $[M+H]^+$ 392.1529, found 392.1545.

*5.1.3.4. 1-(3-Chlorobenzyl)-N-((tetrahydrofuran-3-yl)methyl)-1H-pyrrolo[3,2-c]quinolin-4-amine (**12**).* White solid, yield 45%, t_R = 5.18 min, Mp 169–170 °C, $C_{23}H_{22}ClN_3O$, MW 391.90. ^{1}H NMR (500 MHz, methanol-d_4) δ ppm 1.77–1.86 (m, 1H), 2.12–2.21 (m, 1H), 2.77–2.87 (m, 1H), 3.62–3.68 (m, 2H), 3.71 (dd, J = 8.6, 5.2 Hz, 1H), 3.75–3.82 (m, 1H), 3.88–3.97 (m, 2H), 5.82 (s, 2H), 6.94 (dt, J = 7.3, 1.6 Hz, 1H), 6.99 (d, J = 3.2 Hz, 1H), 7.03 (d, J = 1.8 Hz, 1H), 7.11 (td, J = 7.7, 7.0, 1.3 Hz, 1H), 7.22–7.29 (m, 2H), 7.33 (d, J = 3.2 Hz, 1H), 7.38 (ddd, J = 8.4, 7.0, 1.4 Hz, 1H), 7.78 (dd, J = 8.4, 1.3 Hz, 1H), 7.83 (dd, J = 8.3, 1.4 Hz, 1H). ^{13}C NMR (126 MHz, methanol-d_4) δ ppm 30.91, 40.13, 44.93, 53.20, 66.75, 68.56, 72.36, 102.57, 113.40, 116.33, 121.78, 123.18, 125.21, 126.84, 127.79, 128.57, 130.47, 131.37, 134.74, 135.82, 141.21, 153.22. Monoisotopic mass 391.15, $[M+H]^+$ = 392.7. HRMS (ESI): *m/z* calculated for $[M+H]^+$ 392.1529, found 392.1528.

*5.1.3.5. 2-((1-(3-Chlorobenzyl)-1H-pyrrolo[3,2-c]quinolin-4-yl)(methyl)amino)ethan-1-ol (**24**).* White oil, yield 50%, t_R = 1.39 min, $C_{21}H_{20}ClN_3O$, MW 365.86. ^{1}H NMR (500 MHz, methanol-d_4) δ (ppm) 3.52 (s, 3H), 3.89–3.96 (m, 4H), 5.81 (s, 2H), 6.90–6.94 (m, 1H), 6.98–7.00 (m, 1H), 7.04 (d, J = 3.3 Hz, 1H), 7.08 (ddd, J = 8.3, 7.0, 1.3 Hz, 1H), 7.19–7.26 (m, 2H), 7.32–7.37 (m, 2H), 7.62 (dd, J = 8.3, 1.3 Hz, 1H), 7.84 (dd, J = 8.3, 1.3 Hz, 1H). ^{13}C NMR (126 MHz, methanol-d_4) δ ppm 30.76, 39.96, 53.57, 56.13, 61.84, 105.89, 113.78, 116.17, 121.93, 123.46, 125.38, 125.55, 127.00, 128.14, 128.75, 130.33, 131.56, 136.00, 136.64, 141.30, 155.50. Monoisotopic mass 365.13, $[M+H]^+$ = 366.1. HRMS (ESI): *m/z* calculated for $[M+H]^+$ 366.1373, found 366.1379.

*5.1.4. General procedure for preparation of compounds **13**–**23** and **25**–**33***

Compound **8** (1.7 mmol, 1 eq) was dissolved in acetonitrile followed by addition of TEA (5.1 mmol, 3 eq) and respective amine (6.8 mmol, 4 eq). The reaction was heated in a microwave reactor at 140 °C for 7 h. The solvent was evaporated and the crude product was purified by chromatography using silica gel with CH_2Cl_2/MeOH as a developing solvent.

*5.1.4.1. 1-Benzyl-4-(4-methoxypiperidin-1-yl)-1H-pyrrolo[3,2-c]quinoline (**13**).* White oil, yield 65%, t_R = 1.29, $C_{24}H_{25}N_3O$, MW 371.47. ^{1}H NMR (500 MHz, dmso-d_6) δ ppm 1.54–1.63 (m, 2H), 1.98–2.05 (m, 2H), 3.25–3.31 (m, 5H), 3.40–3.47 (m, 1H), 4.09 (dt, J = 13.4, 4.5 Hz, 2H), 5.88 (s, 2H), 6.79 (d, J = 3.2 Hz, 1H), 7.01 (d, J = 7.5 Hz, 2H), 7.07–7.12 (m, 1H), 7.22 (t, J = 7.3 Hz, 1H), 7.27–7.31 (m, 2H), 7.32–7.36 (m, 1H), 7.54 (d, J = 3.2 Hz, 1H), 7.66 (d, J = 8.2 Hz, 1H), 7.93 (d, J = 8.2 Hz, 1H). ^{13}C NMR (126 MHz, dmso-d_6) δ ppm 30.76, 45.63, 52.30, 54.95, 76.10, 102.64, 113.47, 115.73, 120.58, 122.10, 125.77, 125.98, 127.28, 128.81, 129.45, 134.34, 138.03, 143.77, 154.50. Monoisotopic mass 371.20, $[M+H]^+$ = 372.2. HRMS (ESI): *m/z* calculated for $[M+H]^+$ 372.2076, found 372.2064.

*5.1.4.2. 1-(3-Chlorobenzyl)-4-(4-methoxypiperidin-1-yl)-1H-pyrrolo[3,2-c]quinoline (**14**).* White oil, yield 72%, t_R = 5.42 min, $C_{24}H_{24}ClN_3O$, MW 405.93. ^{1}H NMR (500 MHz, dmso-d_6) δ ppm 1.50–1.69 (m, 1H), 1.75–1.89 (m, 2H), 2.10–2.20 (m, 2H), 3.34–3.41 (m, 1H), 3.43 (s, 3H), 3.46–3.56 (m, 1H), 4.25 (dt, J = 13.4, 4.5 Hz, 2H), 5.71 (s, 2H), 6.75 (d, J = 3.2 Hz, 1H), 6.88–6.93 (m, 1H), 7.06–7.10 (m, 2H), 7.14 (ddd, J = 8.4, 7.0, 1.4 Hz, 1H), 7.20–7.25 (m, 2H), 7.41 (ddd, J = 8.3, 7.0, 1.3 Hz, 1H), 7.77 (ddd, J = 8.3, 1.4, 0.6 Hz, 1H), 7.88 (s, 1H). ^{13}C NMR (126 MHz, dmso-d_6) δ ppm 30.84, 45.71, 51.76, 54.99, 76.20, 102.98, 113.66, 115.70, 120.46, 122.31, 124.57, 125.75, 126.20, 127.41, 127.52, 129.45, 130.84, 133.60, 134.35, 140.83, 143.94, 154.59. Monoisotopic mass 405.16, $[M+H]^+$ = 406.3. HRMS (ESI): *m/z* calculated for $[M+H]^+$ 406.1686, found 406.1683.

*5.1.4.3. 1-(3-Methoxybenzyl)-4-(4-methoxypiperidin-1-yl)-1H-pyrrolo[3,2-c]quinoline (**15**).* White solid, yield 47%, t_R = 5.11 min, Mp 122–124 °C, $C_{25}H_{27}N_3O_2$, MW 401.51. ^{1}H NMR (500 MHz, $CDCl_3$) δ ppm 1.51–1.78 (m, 4H), 2.80–2.87 (m, 1H), 2.90–3.01 (m, 4H), 3.40 (s, 3H), 3.61 (s, 3H), 5.80 (s, 2H), 6.40–6.51 (m, 1H), 6.55 (s, 1H), 6.72 (d, J = 3.1 Hz, 2H), 7.01–7.09 (m, 1H), 7.17 (s, 1H), 7.31 (s, 1H), 7.46–7.51 (m, 1H), 7.58–7.64 (m, 1H), 7.85–7.92 (m, 1H). ^{13}C NMR (126 MHz, dmso-d_6) δ ppm 30.80, 45.69, 52.26, 55.02, 76.16, 102.67, 112.04, 112.19, 113.50, 115.80, 117.91, 120.65, 122.20, 126.07, 127.40, 129.49, 130.05, 134.43, 138.49, 139.75, 143.85, 147.80, 154.57, 159.63. Monoisotopic mass 401.21 $[M+H]^+$ = 402.4. HRMS (ESI): *m/z* calculated for $[M+H]^+$ 402.2181, found 402.2171.

*5.1.4.4. 1-(3-Chlorobenzyl)-4-(3-methoxypiperidin-1-yl)-1H-pyrrolo[3,2-c]quinoline (**16**).* White solid, yield 31%, t_R = 5.49 min, Mp 114–115 °C, $C_{24}H_{24}ClN_3O$, MW 405.93. ^{1}H NMR (500 MHz, $CDCl_3$) δ ppm 1.50–1.55 (m, 1H), 1.77 (dd, J = 10.3, 3.2 Hz, 1H), 1.90–2.01 (m, 1H), 2.15 (dd, J = 12.3, 4.1 Hz, 1H), 3.25 (s, 2H), 3.49 (s, 3H), 3.55–3.62 (m, 1H), 4.12–4.21 (m, 1H), 4.45 (d, J = 11.7 Hz, 1H), 5.71 (s, 2H), 6.79 (s, 1H), 6.91 (dd, J = 2.9, 1.8 Hz, 1H), 7.08 (d, J = 2.3 Hz, 2H), 7.14 (s, 1H), 7.22–7.26 (m, 2H), 7.42 (t, J = 7.3 Hz, 1H), 7.77 (d, J = 8.8 Hz, 1H), 7.85–7.93 (m, 1H). ^{13}C NMR (126 MHz, $CDCl_3$) δ ppm 23.60, 30.66, 49.17, 52.90, 56.51, 75.86, 120.14, 122.80, 124.22, 126.20, 128.22, 130.54, 135.25, 135.61. Monoisotopic mass 405.16, $[M+H]^+$ = 406.2. HRMS (ESI): *m/z* calculated for $[M+H]^+$ 406.1686, found 406.1691.

*5.1.4.5. 1-(3-Chlorobenzyl)-4-(3-methoxypyrrolidin-1-yl)-1H-pyrrolo[3,2-c]quinoline (**17**).* White oil, yield 44%, t_R = 5.35 min, $C_{23}H_{22}ClN_3O$, MW 391.90. ^{1}H NMR (500 MHz, $CDCl_3$) δ ppm 2.04–2.32 (m, 3H), 3.42 (s, 3H), 4.09–4.20 (m, 4H), 5.71 (s, 2H), 6.89 (dt, J = 7.5, 1.2 Hz, 1H), 6.99 (d, J = 282 Hz, 1H), 7.03 (d, J = 1.8 Hz, 1H), 7.11–7.18 (m, 1H), 7.22–7.29 (m, 2H), 7.33 (d, J = 2.3 Hz, 1H), 7.38 (ddd, J = 8.4, 7.1, 1.2 Hz, 1H), 7.54–7.78 (m, 1H), 7.83 (dd, J = 8.3, 1.4 Hz, 1H). ^{13}C NMR (126 MHz, dmso-d_6) δ ppm 30.17, 46.92, 51.88, 53.85, 55.91, 78.95, 104.14, 112.09, 114.35, 120.63, 124.55, 125.69, 126.58, 127.42, 129.35, 130.83, 133.63, 133.96, 140.69. Monoisotopic mass 391.15, $[M+H]^+$ = 391.8. HRMS (ESI): *m/z* calculated for $[M+H]^+$ 392.1529, found 392.1530.

*5.1.4.6. 6-(1-(3-Chlorobenzyl)-1H-pyrrolo[3,2-c]quinolin-4-yl)-2-oxa-6-azaspiro[3.3]heptane (**18**).* White oil, yield 39%, $t_R = 5.30$ min, $C_{23}H_{20}ClN_3O$, MW 389.88.^{1}H NMR (500 MHz, methanol-d_4) δ ppm 3.83–3.90 (m, 4H), 4.42–4.72 (m, 4H), 5.76 (s, 2H), 6.89–6.93 (m, 1H), 6.94 (d, $J = 3.3$ Hz, 1H), 6.96–6.98 (m, 1H), 7.25–7.29 (m, 3H), 7.30 (d, $J = 3.4$ Hz, 1H), 7.49–7.54 (m, 1H), 7.78 (dd, $J = 8.3$, 1.2 Hz, 1H), 8.11 (dd, $J = 8.5$, 1.2 Hz, 1H). ^{13}C NMR (126 MHz, dmso-d_6) δ 38.81, 52.19, 60.85, 80.09, 101.56, 111.55, 115.26, 120.69, 121.20, 125.73, 126.03, 126.60, 127.26, 128.77, 129.57, 133.56, 138.02, 144.52, 153.82. Monoisotopic mass 389.13, $[M+H]^+ = 390.1$. HRMS (ESI): *m/z* calculated for $[M+H]^+$ 390.1373, found 390.1375.

*5.1.4.7. 6-(1-Benzyl-1H-pyrrolo[3,2-c]quinolin-4-yl)-2-oxa-6-azaspiro[3.4]octane (**19**).* White oil, yield 46%, $t_R = 4.70$ min, $C_{24}H_{23}N_3O$, MW 369.47. ^{1}H NMR (500 MHz, dmso-d_6) δ ppm 2.25 (t, $J = 6.8$ Hz, 2H), 3.84 (t, $J = 6.9$ Hz, 2H), 4.05 (s, 2H), 4.52 (d, $J = 6.0$ Hz, 2H), 4.63 (d, $J = 5.9$ Hz, 2H), 5.83 (s, 2H), 6.89–7.02 (m, 4H), 7.18 (d, $J = 7.3$ Hz, 1H), 7.24 (td, $J = 7.5$, 4.5 Hz, 3H), 7.47 (d, $J = 3.2$ Hz, 1H), 7.54 (d, $J = 8.3$ Hz, 1H), 7.83 (d, $J = 8.2$ Hz, 1H). ^{13}C NMR (126 MHz, dmso-d_6) δ ppm 34.60, 41.63, 44.55, 47.23, 51.57, 52.37, 53.45, 57.06, 79.07, 79.76, 79.80, 103.35, 112.16, 114.63, 120.62, 125.74, 126.09, 127.25, 128.77, 129.05, 134.02, 138.02, 151.37, 160.81. Monoisotopic mass 369.18, $[M+H]^+ = 370.2$. HRMS (ESI): *m/z* calculated for $[M+H]^+$ 370.1919, found 370.1908.

*5.1.4.8. 6-(1-(3-Chlorobenzyl)-1H-pyrrolo[3,2-c]quinolin-4-yl)-2-oxa-6-azaspiro[3.4]octane (**20**).* White oil, yield 40%, $t_R = 4.81$ min, $C_{24}H_{22}ClN_3O$, MW 403.91. ^{1}H NMR (500 MHz, dmso-d_6) δ ppm 2.28–2.33 (m, 2H), 3.90–3.01 (m, 2H), 3.10–3.17 (m, 3H), 3.58 (m, 1H), 3.67–3.71 (m, 2H), 5.97 (s, 2H), 6.91 (dt, $J = 7.5$, 1.6 Hz, 1H), 7.06 (t, $J = 2.0$ Hz, 1H), 7.25–7.35 (m, 4H), 7.51 (ddd, $J = 8.4$, 7.1, 1.2 Hz, 1H), 7.76 (d, $J = 3.3$ Hz, 1H), 7.93 (dd, $J = 8.4$, 1.3 Hz, 1H), 8.31 (s, 1H). ^{13}C NMR (126 MHz, dmso-d_6) δ ppm 29.04, 30.30, 44.18, 48.03, 48.85, 49.11, 52.07, 62.20, 107.32, 110.03, 112.81, 118.79, 121.50, 124.50, 125.71, 127.69, 128.60, 130.92, 131.73, 133.45, 133.64, 139.39, 147.38, 160.95. Monoisotopic mass 403.15, $[M+H]^+ = 404.2$. HRMS (ESI): *m/z* calculated for $[M+H]^+$ 404.1529, found 404.1280.

*5.1.4.9. 1-(1-(3-Chlorobenzyl)-1H-pyrrolo[3,2-c]quinolin-4-yl)piperidin-4-ol (**21**).* White oil, yield 45%, $t_R = 4.72$ min, $C_{23}H_{22}ClN_3O$, MW 391.89. ^{1}H NMR (500 MHz, methanol-d_4) δ ppm 1.67–1.83 (m, 2H), 2.07 (dd, $J = 13.1$, 4.0 Hz, 2H), 3.32–3.37 (m, 2H), 3.81–3.95 (m, 1H), 4.18–4.30 (m, 2H), 5.79 (s, 2H), 6.79 (d, $J = 3.2$ Hz, 1H), 6.86–6.95 (m, 1H), 7.02–7.08 (m, 1H), 7.12 (ddd, $J = 8.3$, 7.0, 1.3 Hz, 1H), 7.18–7.27 (m, 2H), 7.31 (d, $J = 3.2$ Hz, 1H), 7.37 (ddd, $J = 8.4$, 7.0, 1.4 Hz, 1H), 7.78 (ddd, $J = 8.4$, 1.4, 0.5 Hz, 1H), 7.86 (ddd, J $J = 8.3$, 1.4, 0.6 Hz, 1H). ^{13}C NMR (126 MHz, methanol-d_4) δ ppm 34.83, 48.11, 53.89, 66.47, 107.76, 112.40, 115.03, 119.76, 123.08, 125.49, 126.54, 127.03, 129.19, 130.37, 131.80, 133.18, 135.41, 136.19, 137.24, 140.04, 151.69. Monoisotopic mass 391.15, $[M+H]^+ = 392.5$. HRMS (ESI): *m/z* calculated for $[M+H]^+$ 392.1529, found 392.1534.

*5.1.4.10. 1-(1-(3-Methoxybenzyl)-1H-pyrrolo[3,2-c]quinolin-4-yl) piperidin-4-ol (**22**).* White oil, yield 47%, $t_R = 4.72$ min, $C_{24}H_{25}N_3O_2$, MW 387.48. ^{1}H NMR (500 MHz, methanol-d_4) δ ppm 1.68–1.85 (m, 2H), 2.00–2.12 (m, 2H), 3.66 (s, 3H), 3.84–3.93 (m, 1H), 4.24 (dt, $J = 14.3$, 4.6 Hz, 2H), 4.55–4.67 (m, 1H), 5.75 (s, 2H), 6.56–6.60 (m, 2H), 6.75–6.79 (m, 2H), 7.09–7.14 (m, 1H), 7.15–7.20 (m, 1H), 7.30 (d, $J = 3.2$ Hz, 1H), 7.34–7.38 (m, 1H), 7.78 (dd, $J = 8.4$, 1.3 Hz, 1H), 7.91 (dd, $J = 8.3$, 1.4 Hz, 1H). ^{13}C NMR (126 MHz, methanol-d_4) δ ppm 35.62, 47.71, 53.97, 55.57, 69.18, 104.08, 112.79, 113.70, 115.47, 117.45, 119.11, 121.94, 123.69, 127.37, 127.79, 130.23, 131.06, 136.69, 140.63, 145.19, 156.89, 161.70. Monoisotopic mass 387.19, $[M+H]^+ = 388.2$. HRMS (ESI): *m/z* calculated for $[M+H]^+$ 388.2025, found 388.2031.

*5.1.4.11. 1-(1-(3-Chlorobenzyl)-1H-pyrrolo[3,2-c]quinolin-4-yl)piperidin-3-ol (**23**).* White oil, yield 89%, $t_R = 4.64$ min, $C_{23}H_{22}ClN_3O$, MW 391.89. ^{1}H NMR (500 MHz, $CDCl_3$/methanol-d_4) δ ppm 1.70–1.82 (m, 2H), 2.06–2.18 (m, 2H), 3.97–4.08 (m, 1H), 4.26 (m, 2H), 4.58–4.69 (m, 2H), 5.74 (s, 2H), 6.87–6.95 (m, 1H), 6.98 (d, $J = 3.4$ Hz, 1H), 7.05 (d, $J = 2.5$ Hz, 1H), 7.11 (ddd, $J = 8.3$, 7.0, 1.3 Hz, 1H), 7.19–7.26 (m, 2H), 7.33–7.38 (m, 2H), 7.62–7.73 (m, 1H), 7.83 (dd, $J = 8.3$, 1.4 Hz, 1H). ^{13}C NMR (126 MHz, dmso-d_6) δ ppm 23.26, 33.58, 47.99, 52.30, 55.48, 65.76, 102.70, 113.43, 115.68, 120.58, 121.99, 125.77, 126.01, 127.17, 127.28, 128.81, 129.39, 134.36, 138.03, 143.79, 154.54. Monoisotopic mass 391.15, $[M+H]^+ = 392.2$. HRMS (ESI): *m/z* calculated for $[M+H]^+$ 392.1529, found 392.1534.

*5.1.4.12. 1-(3-Chlorobenzyl)-4-(piperidin-1-yl)-1H-pyrrolo[3,2-c] quinoline (**25**).* White oil, yield 65%, $t_R = 5.86$ min, $C_{23}H_{22}ClN_3$, MW 375.90. ^{1}H NMR (500 MHz, $CDCl_3$) δ ppm 1.73–1.79 (m, 2H), 1.80–1.87 (m, 4H), 3.66–3.97 (m, 4H), 5.71 (s, 2H), 6.72–6.80 (m, 1H), 6.91 (dt, $J = 6.5$, 2.0 Hz, 1H), 7.04–7.11 (m, 2H), 7.09–7.18 (m, 1H), 7.18–7.27 (m, 2H), 7.42 (t, $J = 7.6$ Hz, 1H), 7.75 (dd, $J = 8.4$, 1.4 Hz, 1H), 7.89 (s, 1H). ^{13}C NMR (126 MHz, dmso-d_6) δ ppm 24.54, 25.71, 49.20, 51.72, 120.50, 122.35, 124.53, 125.70, 126.34, 127.39, 130.82, 133.53, 134.29. Monoisotopic mass 375.15, $[M+H]^+ = 376.4$. HRMS (ESI): *m/z* calculated for $[M+H]^+$ 376.1502, found 376.1578.

*5.1.4.13. 1-(3-Chlorobenzyl)-4-(4,4-difluoropiperidin-1-yl)-1H-pyrrolo[3,2-c]quinoline (**26**).* White oil, yield 84%, $t_R = 5.37$ min, $C_{23}H_{20}ClF_2N_3$, MW 411.87. ^{1}H NMR (500 MHz, dmso-d_6) δ ppm 2.20–2.44 (m, 4H), 3.98–4.34 (m, 4H), 6.03 (s, 2H), 6.93–7.01 (m, 1H), 7.14 (d, $J = 2.0$ Hz, 1H), 7.26 (s, 1H), 7.30–7.41 (m, 2H), 7.38–7.45 (m, 1H), 7.62 (t, $J = 7.7$ Hz, 1H), 7.82–7.89 (m, 1H), 8.06 (d, $J = 8.4$ Hz, 1H), 8.36 (s, 1H). ^{13}C NMR (126 MHz, dmso-d_6) δ ppm 33.63, 46.72, 52.14, 106.70, 113.48, 121.69, 122.28, 124.62, 125.38, 125.86, 127.83, 128.97, 131.00, 132.49, 133.80, 135.20, 139.38. Monoisotopic mass 411.13, $[M+H]^+ = 412.1$. HRMS (ESI): *m/z* calculated for $[M+H]^+$ 412.1392, found 412.1398.

*5.1.4.14. 1-Benzyl-4-(4,4-difluoropiperidin-1-yl)-1H-pyrrolo[3,2-c] quinoline (**27**).* White oil, yield 90%, $t_R = 5.35$ min, $C_{23}H_{21}F_2N_3$, MW 377.43. ^{1}H NMR (500 MHz, $CDCl_3$) δ ppm 2.14–2.28 (m, 4H), 3.89–3.98 (m, 4H), 5.76 (s, 2H), 6.71 (d, $J = 3.2$ Hz, 1H), 7.05–7.09 (m, 2H), 7.11 (d, $J = 3.2$ Hz, 1H), 7.17 (ddd, $J = 8.3$, 7.0, 1.3 Hz, 1H), 7.27–7.34 (m, 3H), 7.43 (ddd, $J = 8.3$, 7.0, 1.4 Hz, 1H), 7.85–7.90 (m, 2H). ^{13}C NMR (126 MHz, dmso-d_6) δ ppm 33.61, 46.83, 52.68, 106.45, 110.89, 113.47, 121.74, 122.25, 125.15, 125.80, 127.67, 128.70, 128.98, 132.49, 135.16, 136.64, 150.20. Monoisotopic mass 377.17, $[M+H]^+ = 378.0$. HRMS (ESI): *m/z* calculated for $[M+H]^+$ 378.1782, found 378.1792.

*5.1.4.15. 4-(4,4-Difluoropiperidin-1-yl)-1-(2-fluorobenzyl)-1H-pyrrolo[3,2-c]quinoline (**28**).* White oil, yield 75%, $t_R = 5.36$ min, $C_{23}H_{20}F_3N_3$, MW 395.43. ^{1}H NMR (500 MHz, dmso-d_6) δ ppm δ (ppm) 2.13–2.28 (m, 4H), 3.82–3.89 (m, 4H), 5.94 (s, 2H), 6.28 (dd, $J = 7.8$, 1.6 Hz, 1H), 6.92 (d, $J = 3.3$ Hz, 1H), 7.13–7.19 (m, 2H), 7.33 (td, $J = 7.7$, 1.6 Hz, 1H), 7.39 (ddd, $J = 8.2$, 7.1, 1.4 Hz, 1H), 7.59 (d, $J = 3.2$ Hz, 1H), 7.61 (dd, $J = 8.0$, 1.2 Hz, 1H), 7.68 (dd, $J = 8.5$, 1.3 Hz, 1H), 7.75 (dd, $J = 8.2$, 1.3 Hz, 1H).^{13}C NMR (126 MHz, dmso-d_6) δ ppm 33.56, 44.99, 47.06, 47.10, 102.34, 102.77, 115.67, 117.55, 120.21, 120.88, 126.43, 127.17, 128.99, 131.79, 134.29, 134.55, 143.23, 143.56, 144.40, 153.77, 158.33, 160.28. Monoisotopic mass 395.16, $[M+H]^+ = 396.2$. HRMS (ESI): *m/z* calculated for $[M+H]^+$ 378.1782, found 378.1792. HRMS (ESI): *m/z* calculated for $[M+H]^+$ 396.1687, found 396.1678.

*5.1.4.16. 1-(2-Chlorobenzyl)-4-(4,4-difluoropiperidin-1-yl)-1H-pyrrolo[3,2-c]quinoline (**29**).* White oil, yield 72%, t_R = 5.37 min, $C_{23}H_{20}ClF_2N_3$, MW 411.88. ^{1}H NMR (500 MHz, dmso-d_6) δ (ppm) 2.12−2.26 (m, 4H), 3.80−3.88 (m, 4H), 5.92 (s, 2H), 6.27 (dd, J = 7.8, 1.6 Hz, 1H), 6.90 (d, J = 3.2 Hz, 1H), 7.11−7.17 (m, 2H), 7.30 (td, J = 7.7, 1.6 Hz, 1H), 7.38 (ddd, J = 8.3, 7.0, 1.3 Hz, 1H), 7.58 (d, J = 3.2 Hz, 1H), 7.60 (dd, J = 8.0, 1.2 Hz, 1H), 7.66 (dd, J = 8.5, 1.3 Hz, 1H), 7.73 (dd, J = 8.3, 1.3 Hz, 1H). ^{13}C NMR (126 MHz, dmso-d_6) δ ppm 33.56, 44.97, 50.63, 102.88, 113.38, 115.85, 119.80, 122.74, 126.22, 126.81, 127.71, 127.87, 129.29, 129.44, 129.57, 130.95, 134.46, 135.05, 143.58, 153.75. Monoisotopic mass 411.13, $[M+H]^+$ = 412.1. HRMS (ESI): *m/z* calculated for $[M+H]^+$ 412.1392, found 412.1392.

*5.1.4.17. 4-(4,4-Difluoropiperidin-1-yl)-1-(3-fluorobenzyl)-1H-pyrrolo[3,2-c]quinoline (**30**).* White oil, yield 84%, t_R = 5.37 min, $C_{23}H_{20}F_3N_3$, MW 395.43. ^{1}H NMR (500 MHz, dmso-d_6) δ ppm 2.30−2.42 (m, 4H), 4.13−4.21 (m, 4H), 6.04 (s, 2H), 6.80−6.88 (m, 1H), 6.89 (dt, J = 10.1, 2.0 Hz, 1H), 7.05−7.15 (m, 1H), 7.27 (d, J = 3.2 Hz, 1H), 7.32−7.46 (m, 2H), 7.63 (t, J = 7.8 Hz, 1H), 7.87 (d, J = 3.3 Hz, 1H), 8.06 (dd, J = 8.5, 1.3 Hz, 1H), 8.34 (s, 1H).^{13}C NMR (126 MHz, dmso-d_6) δ ppm 33.59, 46.72, 52.20, 66.43, 106.64, 112.78, 112.96, 114.54, 114.70, 121.68, 121.88, 125.33, 128.91, 131.14, 131.21, 132.49, 135.16, 139.73, 161.56, 163.51. Monoisotopic mass 395.16, $[M+H]^+$ = 396.2. HRMS (ESI): *m/z* calculated for $[M+H]^+$ 396.1687, found 396.1686.

*5.1.4.18. 4-(4,4-Difluoropiperidin-1-yl)-1-(3-methoxybenzyl)-1H-pyrrolo[3,2-c]quinoline (**31**).* White solid, yield 82%, t_R = 5.37 min, Mp 236−237 °C, $C_{24}H_{23}F_2N_3O$, MW 407.47. ^{1}H NMR (500 MHz, $CDCl_3$) δ ppm 2.14−2.29 (m, 4H), 3.72 (s, 3H), 3.88−3.97 (m, 4H), 5.72 (s, 2H), 6.58−6.65 (m, 1H), 6.67 (ddd, J = 7.6, 1.7, 0.9 Hz, 1H), 6.70 (d, J = 3.2 Hz, 1H), 6.80 (ddd, J = 8.3, 2.6, 0.9 Hz, 1H), 7.11 (d, J = 3.2 Hz, 1H), 7.18 (ddd, J = 8.2, 7.0, 1.4 Hz, 1H), 7.24 (t, J = 8.0 Hz, 1H), 7.43 (ddd, J = 8.4, 7.0, 1.3 Hz, 1H), 7.88 (dd, J = 8.3, 1.4 Hz, 2H). ^{13}C NMR (126 MHz, dmso-d_6) δ ppm 33.26, 33.45, 33.63, 46.69, 52.39, 54.91, 106.25, 110.68, 111.95, 112.32, 113.30, 117.60, 121.57, 122.09, 125.00, 128.52, 130.03, 132.30, 135.01, 138.11, 150.02, 159.50. Monoisotopic mass 407.18, $[M+H]^+$ = 408.1. HRMS (ESI): *m/z* calculated for $[M+H]^+$ 408.1887, found 408.1891.

*5.1.4.19. 4-(4,4-Difluoropiperidin-1-yl)-1-(4-fluorobenzyl)-1H-pyrrolo[3,2-c]quinoline (**32**).* White solid, yield 84%, t_R = 5.43 min, Mp 257−258 °C, $C_{23}H_{20}F_3N_3$, MW 395.43. ^{1}H NMR (500 MHz, $CDCl_3$) δ ppm 2.11−2.31 (m, 4H), 3.95 (t, J = 5.3 Hz, 4H), 5.71 (s, 2H), 6.80 (d, J = 8.0 Hz, 2H), 7.02 (d, J = 3.1 Hz, 1H), 7.05 (d, J = 8.1 Hz, 2H), 7.19 (t, J = 7.7 Hz, 1H), 7.43 Hz (d, J = 2.9 Hz, 1H), 7.84 (d, J = 8.2 Hz, 2H). ^{13}C NMR (126 MHz, $CDCl_3$) δ ppm 32.73, 45.52, 50.00, 100.86, 115.40, 116.57, 120.12, 121.90, 126.12, 126.59, 127.17, 130.29, 130.83, 133.05, 133.07, 135.98, 149.43, 152.35, 161.23. Monoisotopic mass 395.16, $[M+H]^+$ = 396.2. HRMS (ESI): *m/z* calculated for $[M+H]^+$ 396.1687, found 396.1694.

*5.1.4.20. 1-(4-Chlorobenzyl)-4-(4,4-difluoropiperidin-1-yl)-1H-pyrrolo[3,2-c]quinoline (**33**).* White solid, yield 87%, t_R = 5.87 min, Mp 243−245 °C, $C_{23}H_{20}ClF_2N_3$, MW 411.88. ^{1}H NMR (500 MHz, $CDCl_3$) δ ppm 2.13−2.33 (m, 4H), 3.90−3.99 (m, 4H), 5.71 (s, 2H), 6.82 (d, J = 8.0 Hz, 2H), 7.06 (d, J = 3.1 Hz, 1H), 7.04 (d, J = 8.1 Hz, 2H), 7.21 (t, J = 7.7 Hz, 1H), 7.44 Hz (d, J = 2.9 Hz, 1H), 7.85 (d, J = 8.2 Hz, 2H). ^{13}C NMR (125 MHz, $CDCl_3$) δ ppm 32.73, 45.52, 50.12, 100.90, 115.95, 116.68, 121.93, 126.12, 127.16, 127.31, 128.77, 129.39, 130.85, 132.76, 135.61, 135.98, 149.46, 152.35. Monoisotopic mass 411.13, $[M+H]^+$ = 412.1. HRMS (ESI): *m/z* calculated for $[M+H]^+$ 412.1392, found 412.1382.

5.2. In silico evaluation

5.2.1. Evaluation of water positions

Five complexes (PDB ID: 2v60,[37] 2v61,[37] 2v5z [37], 6fw0,[38] and 6fwc [38]) of MAO-B, crystalized with non-covalent inhibitors (which contain F or Cl atom in phenyl ring) were selected from the protein data bank (PDB) [39]. Each complex contained water molecules close to the ligand. To select the conserved water molecules in the binding site, an alignment of all complexes was performed using SiteMap with aligning residues within 5 Å from the ligand [40,41]. It was found, that four water molecules localized close to the FAD molecule, and three water molecules in the binding crevice formed by ILE199, GLN206, and TYR326 had common positions.

5.2.2. Induced fit docking

The 3-dimensional structures of the ligands were prepared using LigPrep v3.6[42] and the appropriate ionization states at pH = 7.0 ± 0.5 were assigned using Epik v3.4 [43,44]. Compounds with unknown absolute configuration were docked in R and S configurations. The Protein Preparation Wizard [45] was used to assign the bond orders, appropriate amino acid ionization states, and to check for steric clashes for the MAO-B crystals. The water molecules, except those that were chosen as conserved, were removed. The receptor grid was generated (OPLS3 force field) [46−48] by centering the grid box with a size of 8 Å on non-covalently bonded inhibitors. Automated flexible docking was performed using Glide v6.9[49−51] at the SP level.

5.2.3. Molecular dynamics

The starting conformation of the L-R complexes were carefully selected for each ligand with a binding mode similar to the one observed in the crystal structure and which value of the RMSF of oxygen atoms in water molecules was the smallest. A 50 ns-long Molecular Dynamics (MD) simulations were performed using Schrödinger Desmond software. The system was solvated by water molecules described by the TIP4P potential and the OPLS3 force field parameters were used for all atoms. 0.15 M NaCl was added to mimic the ionic strength inside the cell. The output trajectories were hierarchically clustered into 5 clusters according to the ligand using trajectory analysis tools available in the Maestro Schrödinger Suit.

5.2.4. Quantum polarized ligand docking

The top-three **26**-MAO-B complex clusters were selected and used as a grid for the next steps. The receptor grids were generated (OPLS3 force field) by centering the grid box with a size of 8 Å on the **26** compound. Docking was performed by quantum-polarized ligand docking (QPLD) procedure [52] involves the QM-derived ligand atomic charges in the protein environment at the 3-21G/BLYP level. For each ligand, the 5 poses were obtained.

5.2.5. Binding free energy calculations

GBSA (Generalized-Born/Surface Area) was used to calculate the binding free energy based on the ligand−receptor complexes generated by the QPLD procedure. The ligand poses were minimized using the local optimization feature in Prime, the flexible residue distance was set to 6 Å from a ligand pose, and the ligand charges obtained in the QPLD stage were used. The energies of complexes were calculated with the OPLS3e force field and Generalized-Born/Surface Area continuum solvent model. To assess the influence of a given substituent on the binding, the ΔΔG was calculated as a difference between binding free energy (ΔG) of the unsubstituted phenyl ring and its halogenated analog.

5.3. In vitro pharmacological evaluation

5.3.1. 5-HT_6Rs affinity evaluation

5.3.1.1. Cell culture and preparation of cell membranes for radioligand binding assays. HEK293 cells with stable expression of human 5-HT_6, receptors (prepared with the use of Lipofectamine 2000) were maintained at 37 °C in a humidified atmosphere with 5% CO_2 and grown in Dulbecco's modified Eagle medium containing 10% dialyzed fetal bovine serum and 500 μg/ml G418 sulfate. For membrane preparation, cells were sub-cultured in 150 cm^2 flasks, grown to 90% confluence, washed twice with phosphate buffered saline (PBS) prewarmed to 37 °C, and pelleted by centrifugation (200×*g*) in PBS containing 0.1 mM EDTA and 1 mM dithiothreitol. Prior to membrane preparation, pellets were stored at −80 °C.

5.3.1.2. Radioligand binding assays. The cell pellets were thawed and homogenized in 10 vol of assay buffer using an Ultra Turrax tissue homogenizer, centrifuged twice at 35000×*g* for 15 min at 4 °C, and incubated for 15 min at 37 °C between centrifugation rounds. The composition of the assay buffers was 50 mM Tris HCl, 0.5 mM EDTA, and 4 mM $MgCl_2$. The assays were incubated in a total volume of 200 μL in 96-well microtiter plates for 1 h at 37 °C. The process of equilibration was terminated by rapid filtration through Unifilter plates with a 96-well cell harvester, and radioactivity retained on the filters was quantified on a Microbeta plate reader (PerkinElmer, USA). For displacement studies, the assay samples contained as radioligands (PerkinElmer, USA) 2 nM [^{3}H]-LSD (83.6 Ci/mmol). Nonspecific binding was defined with 10 μM methiothepine. Each compound was tested in triplicate at 7 concentrations (10^{-10} to 10^{-4} M). The inhibition constants (K_i) were calculated from the Cheng−Prusoff equation [53]. Results were expressed as means of at least two independent experiments.

5.3.2. Monoamine oxidase assays

Inhibition activity of evaluated compounds was measured using human recombinant MAO-B and MAO-A (Sigma Aldrich M7441 and M7316) in the fluorometric method for detecting monoamine oxidase activity. The assay was carried out in a 96-well plate. 2 μl of the appropriate concentration of tested compounds in DMSO were added to wells that contained 98 μl of enzyme dilution (0.53 U/ml) in phosphate buffer (50 mM, pH 7.4). After the 30 min of pre-incubation at room temperature 50 μl of the solution of 800 μM10-Acetyl-3,7 dihydroxyphenoxazine (Cayman Chemical Company 10010469) and 4 U/ml horse radish peroxidase (HRP, Sigma Aldrich P6782) was added and enzymatic reaction was started by addition of 50 μl of 800 μM *p*-tyramine (Alfa Aesar A12220) solution. The signal was measured after 1 h (excitation at 570 nm and emission at 585 nm) using EnSpire® multimode plate reader (PerkinElmer, Inc.). Rasagiline (1 μM) or clorgyline (1 μM) were tested as reference compounds for MAO-B and MAO-A inhibitions, respectively [54,55].

5.3.3. Reversibility studies

To investigate the reversibility of MAO-B inhibition compound **26**, rasagiline and safinamide were tested in concentration corresponding to their IC_{80} values. Experiment was carried out in a 96-well plate. hMAO-B was incubated with inhibitors for 30 min then low concentration of *p*-tyramine (10 μM in wells) and the solution of 10-acetyl-3,7- dihydroxyphenoxazine and HRP (200 μM and 1 U/ml in wells) were added to the plate. Fluorescence signal had been measured in the microplate reader for 22 min then the concentration of *p*-tyramine was increased to 1 mM. After the addition of *p*-tyramine fluorescence was measured every 5 min for 5 h in order to monitor the enzymatic reaction product formation [54−56].

5.3.4. Evaluation of mode of inhibition

The mode of the inhibition was tested according to the standard test procedure using different concentrations of the substrate [56−58]. Inhibitor (compound **26**) was used in three concentrations corresponding to its IC_{20}, IC_{50} and IC_{80} values. Substrate was used in six concentrations: 0.05 nM, 0.1 mM, 0.5 mM, 1 mM, 1.5 mM, 2 mM. After the experiment velocities were calculated and put on the graph (y-axis) against the concentration of the substrate (x-axis). From the Michaelis-Menten plot V_{max}, K_M and α values were calculated for different concentrations of the inhibitor. Double-reciprocal plot (Lineweaver-Burk plot) was prepared to display the data [55−57].

5.4. In vitro metabolic stability studies

Metabolic stability of tested compound was analyzed using incubation systems, composed of: tested compound (10 μM), rat liver microsomes (RLMs, microsomes from rat male liver, pooled; 0.4 mg/ml; Sigma Aldrich), NADPH-regenerating system ($NADP^+$, glucose-6-phosphate and glucose-6-phosphate dehydrogenase in 100 mM potassium buffer, pH 7.4; all from Sigma Aldrich) and potassium buffer, pH 7.4. The stock solution of tested compounds was prepared in methanol (the final methanol concentration in incubation mixture does not exceed 0,1%). Firstly, all samples contained incubation mixture (without NADPH-regenerating system) were pre-incubated in thermoblock at 37 °C, for 10 min. Then the reaction was initiated by the addition of NADPH-regenerating system. In control samples NADPH-regenerating system was replaced with potassium buffer. Probes were incubated for 30 and 60 min at 37 °C. After addition of internal standard (pentoxifylline, 10 mM) biotransformation process was stopped by addition of perchloric acid. Next, samples were centrifuge and supernatants were analyzed using UPLC/MS (Waters Corporation, Milford, MA). All experiments were run in duplicates. Half-life time was evaluated using a non-linear regression model using Graph Pad Prism software and intristinic clearence was calculated from the equation Clint L̆ (volume of incubation [ml]/protein in the incubation [mg]) 0.693/t1/2 [59].

5.5. Assessment of glioprotective properties

5.5.1. Cell culture

Astrocytes (C8-D1A cells, CRL-2541 ATCC) were cultured in 25 cm^2 flask with Dulbecco's Modified Eagle's Medium (DMEM) supplemented with 10% FBS (Fetal Bovine Serum) and 1% pencilin-streptomycin solution at 37 °C, in a humidified atmosphere with 5% CO_2 until the cells reached appropriate confluence. Cells were seeded in 96-well plates at a density of 1* 10^4 cells per well. For protection studies, astrocytes were co-treated with the cytotoxic agent (DOX) and analyzed compounds (26, SAF, SEL) for 24 h; then the ability of compounds to protect astrocytes against DOX-induced toxicity was examined using MTT assay.

5.5.2. MTT assay

Cell viability was estimated by using the MTT assay, which assesses the ability of mitochondrial dehydrogenases to reduce tetrazolium salts into a colored formazan compound [60]. At the end of the incubation period, 10 ml of MTT (5 mg/ml) were added to each well. After 4 h, formazan crystals were solubilized with DMSO and optical density was measured at 570 nm by using a SpectraMax iD3 Multi-Mode Microplate Reader (Molecular Devices). Each experiment was performed in triplicate and repeated three times.

5.6. Inhibition of cytochrome P450

The luminescent CYP3A4, CYP2D6 and CYP2C9 P450-Glo™ assays and protocols were provided by Promega (Madison, WI, USA). The method is based on the conversion the beetle D-luciferin derivative into D-luciferin catalyzed by the respective CYP isoform. After addition of the luciferase, the luminescence signal is produced directly proportional to the amount of obtained by CYP's D-luciferin. The enzymatic reactions were performed in white polystyrene, flat-bottom Nunc™ MicroWell™ 96-well microplates (Thermo Scientific, Waltham, MA USA). The luminescence signal was measured with a microplate reader EnSpire (PerkinElmer, Waltham, MA USA) in luminescence mode. The signal produced without the presence of the tested compound was considered as 100% of CYP activity. The IC_{50} values of reference CYP inhibitors: ketoconazole (3A4), quinidine (2D6) and sulfaphenazole (2C9) were calculated according to the manufacturer's recommendations. Each compound was tested in triplicate at the final concentrations in the range from 0.01 to 25 μM. GraphPad Prism™ software (version 5.01, San Diego, CA, USA) was used to calculate IC_{50} values.

5.7. Evaluation of hepatotoxicity

HepG2 (ATCC® HB-8065™) *hepatoma* cell line was kindly donated by the Department of Pharmacological Screening, Jagiellonian University Medical College. The cells were cultured in Dulbecco's modified Eagle's medium (DMEM) with 10% fetal bovine serum (FBS) (Gibco, Carlsbad, CA, USA. The HepG2 cells were seeded in 96-well transparent plates at a concentration of 1×10^4 cells/well and incubated for 24 h at 37 °C in a 5% CO_2 atmosphere to reach 50% of confluence. Tested compounds were diluted into a fresh growth medium and added to the cells at the final concentrations 0.1 μM−100 μM. The positive controls doxorubicin and mitochondrial toxin CCCP were also added at 1 μM and 10 μM, respectively. The cells were incubated next for 72 h. To asses cells' viability, the MTS reagent (CellTiter 96® AQueous One Solution Cell Proliferation Assay, Promega, Madison, WI, USA) was added to each well. After 4 h of incubation, the absorbance was measured using a microplate reader (EnSpire, PerkinElmer, Waltham, MA USA) at 490 nm. GraphPad Prism™ software (version 5.01, San Diego, CA, USA) was used to calculate statistical significances.

5.8. In vivo pharmacokinetic study

5.8.1. Animals and ethical statement

The purpose of this study was to evaluate the pharmacokinetic profile and distribution to the brain for compound **26** in Sprague-Dawley rats (Charles River Laboratories, Germany) after a single intravenous and intragastric administration of a compound in a dose of 3 mg/kg dissolved in colliphor. The study was performed under the approval of the I Local Ethics Committee for Experiments on Animals of the Jagiellonian University in Krakow, Poland No. 333/2019. During the habituation period the groups of 5 rats were kept in a plastic cage (252 mm × 167 cm x 140 cm) at a controlled room temperature (22 ± 2 °C), humidity (55 ± 10%), full spectrum cold white light (350−400 lx), on 12 h light/dark cycles (the lights on at 7:00 a.m., and off at 19:00 p.m.), and had free access to standard laboratory pellet and tap water.

5.8.2. Sample preparation

A group of 70 Sprague-Dawley rats (Charles River Laboratories, Germany), 13−15 weeks of age and weighing 220−250 g were used in the study. Blood and brain samples were obtained at 7 time points (5 min, 15 min, 30 min, 60 min, 120 min, 240 min, 480 min) after intravenous or intragastric administration of compound **26**. In addition, 5 rats were administered the vehicle of the test substance (colliphor) at t = 0. Rats were anesthetized by i.p. injection of 50 mg/kg ketamine plus 8 mg/kg xylazine, then blood samples have been taken from the right ventricle, and the brain after decapitation. The brain was flushed three times with saline. The plasma was separated by centrifugation (3000×*g*, 10 min), then plasma and brain were stored at −80 °C pending analysis.

The plasma and brain sample pretreatment procedure involved acetonitrile precipitation. A 10 μl aliquot of the IS working solution (5000 ng/ml) was added to 100 μl of the collected rat plasma sample, which was then vortex-mixed for 10 s. Thereafter, 200 μl of cooled acetonitrile was added, vortexed during 20 min, and then centrifuged (3000×*g*, 10 min). The supernatant (200 μl) was then transferred to insert placed in an autosampler vial, and a 20 μl volume of this was injected onto the LC column.

Brain samples were thawed before use, and whole brain were weighted and placed in a glass mortar and pestle tissue grinder, and homogenized with an appropriate amount of phosphate buffer (pH 7.4) in 1:5 ratio. Afterward, 100 μl of tissue homogenates were transferred to new Eppendorf tubes and spiked with 10 μl of the IS working solution (5000 ng/ml).

5.8.3. LC/MS/MS analyses

An ultra-performance liquid chromatography system (Dionex 3000, USA) coupled to mass detection (TSQ Quantum, Thermo Scientific, Germany) was used to determine the concentration of the studied compound. Chromatographic separation of the compound was carried out on a UPLC BEH C18 column (1.7 μm, 3.0 × 100 mm) using as a mobile phase 0.1% formic acid in acetonitrile and 0.1% formic acid in the water, in isocratic elution, at a mobile phase flow rate of 300 μL/min. The ion source parameters were as follows: ion spray voltage: 5000 V; nebulizer gas (gas 1): 20 psi; turbo gas (gas 2): 20 psi; temperature of the heated nebulizer: 400 °C; curtain gas: 10 psi; collision gas: 10 psi. Quantitative analysis was performed in the selected fragmentation reactions (SRM), monitoring the following ions transitions: *m/z* 412.4 (Q1) and *m/z* 125.1, 168.1, 287.2, 291.2, 320.2 (Q3). The internal standard (IS) used was 2-(4-methyl-1-piperazinyl)-4-phenylquinazoline (PH002437), purchased from Sigma-Aldrich, to monitor the ion transition 305.0 (Q1) and 248.0 (Q3).

Basic parameters characterizing the pharmacokinetic profile of **26**, assuming model-independent pharmacokinetics, such as volume of distribution at steady-state, half-life, clearance, mean residence time of the compound in the body, area under the concentration-time curve, maximum concentration, time to reach the maximum concentration were determined from analysis of the concentration of the compound **26** determined at different times after administration (5 min, 15 min, 30 min, 60 min, 120 min, 240 min and 480 min) in plasma and brain homogenates. Pharmacokinetic calculations were performed using Phoenix WinNonlin software (Certara, Princeton, NJ 08540 USA).

First-order elimination rate constant (λ_z) was calculated by linear regression of time versus log concentration. Next, the area under the mean serum and tissue concentration versus time curve ($AUC_{0\rightarrow t}$) was estimated using the log-linear trapezoidal rule, where C_n is the concentration of last sampling of each compound.

$$AUC_{0\rightarrow t} = \sum_{i=1}^{n}((C_i + C_{i+1}) / 2) \cdot (t_{i+1} - t_i) + C_n / \lambda_z \qquad \text{(Eq. 1)}$$

The area under the first-moment curve ($AUMC_{0\rightarrow t}$) was estimated by calculation of the total area under the first-moment curve using equation (2), where t_n is the time of the last sampling.

$$AUMC_{0\to t} = \sum_{i=1}^{n}((t_i \cdot C_i + t_{i+1} \cdot C_{i+1}) / 2) \cdot (t_{i+1} - t_i) + (t_n \cdot C_n) / \lambda_z + C_n / \lambda_z^2 \quad \text{(Eq. 2)}$$

Mean residence time (MRT) was calculated as:

$$MRT = \frac{AUMC_{0\to t}}{AUC_{0\to t}} \quad \text{(Eq. 3)}$$

Total clearance (Cl_T) was calculated as:

$$Cl_T = \frac{F \cdot D_{i.v.}}{AUC_{0\to t}} \quad \text{(Eq. 4)}$$

The volume of distribution at steady-state (V_{ss}) was calculated as:

$$V_{ss} = \frac{D_{iv} \cdot AUMC_{0\to t}}{(AUC_{0\to t})^2} \quad \text{(Eq. 5)}$$

The absolute bioavailability after intragastric administration was calculated as:

$$F(\%) = \frac{AUC_{i.p.}}{AUC_{i.v.}} \cdot \frac{D_{i.v.}}{D_{i.p.}} \cdot 100 \quad \text{(Eq. 6)}$$

where $D_{i.v.}$ and $D_{i.g.}$. are *i.v.* and *i.g.* doses of studied compounds, respectively.

5.9. In vivo pharmacological evaluation

5.9.1. Animals

NOR study: Male Sprague-Dawley rats (Charles River, Germany) weighing 250–280 g on arrival were housed in a temperature-controlled (21 ± 1 °C) and humidity-controlled (40–50%) colony room under a 12/12 h light/dark cycle (lights on at 06:00 h). The rats were group-housed (5/cage) with free access to food and water. Rats could acclimatize for at least 7 days before the start of the experimental procedures. Behavioral testing was performed during the light phase of the light/dark cycle. The experiments were conducted in accordance with the European Guidelines for animal welfare (2010/63/EU) and were approved by the II Local Ethics Committee for Animal Experiments at the Maj Institute of Pharmacology, Polish Academy of Sciences, Krakow, Poland.

FST study: The experiments were performed on male Swiss albino mice (22–26 g) purchased from a licensed breeder Staniszewska (Ilkowice, Poland). The animals were kept in groups of ten to Makrolon type 3 cages (dimensions 26.5 × 15 × 42 cm) in environmentally controlled rooms (ambient temperature 22 ± 2 °C; relative humidity 50–60%; 12:12 light:dark cycle, lights on at 8:00). They were allowed to acclimatize with the environment for one week before commencement of the experiments. Standard laboratory food (Ssniff M-Z) and filtered water were freely available. All the experimental procedures were approved by the I Local Ethics Commission at the Jagiellonian University in Kraków. The experiment was conducted in the light phase between 09.00 and 14.00 h. Each experimental group consisted of: 7–9 animals/dose. The animals were used only once. The experiment was performed by an observer unaware of the treatment administered.

5.9.2. Drugs

Compound **26** was suspended in the mixture of EtOH/colliphor/water (0.05/0.10/0.85; v/v/v) and was administered intraperitoneally (*i.p.*) at a volume of 10 ml/kg, 60 min before the test. Control animals received a vehicle injection.

5.9.3. Novel object recognition test

The test was carried out as described earlier [61]. Briefly, rats were tested in a dimly lit apparatus made of a dull gray plastic (66 × 56 × 30 cm). Following habituation on day 1, two trials separated by an inter-trial interval (ITI) of 1 h were carried out on the day 2. During the first trial (familiarization, T1) two identical objects (A1 and A2) were presented in the opposite corners of the apparatus, approximately 10 cm from the walls. During the second trial (recognition, T2) one of the A objects were replaced by a novel one, so that the animals were presented with the A = familiar and B = novel objects. Both trials lasted for 3 min. Rats were considered exploring objects when looking, licking, sniffing, or touching the object. Exploration time of the objects was measured manually by an experimenter unaware of treatment conditions. Based on exploration time (E) of two objects during T2, discrimination index (DI) was calculated according to the formula: DI = (EB–EA)/(EA + AB).

5.9.4. Forced swim test

The experiment was carried out according to the method of Porsolt et al. [62] Briefly, Swiss albino mice were individually placed in a glass cylinder (25 cm high; 10 cm in diameter) containing 10 cm of water maintained at 23–25 °C, and were left there for 6 min. The total duration of immobility was recorded during the last 4 min of a 6-min test session. A mouse was regarded as immobile when it remained floating on the water, making only small movements to keep its head above it.

5.9.5. Statistics

The data are presented as the mean ± SEM. The statistical significance of the results was evaluated by a one-way ANOVA, followed by Newman-Keuls (NOR study) and Bonferroni's Comparison Test (FST study); $p < 0.05$ was considered significant.

Declaration of competing interest

The authors declare that they have no known competing financial interests or personal relationships that could have appeared to influence the work reported in this paper.

Acknowledgements

The study was financially supported by the National Science Center, Grant No. 2016/21/B/NZ7/01742 and Grant No. 2019/35/N/NZ7/04312, and Innovation Incubator 2.0 project funded by the Ministry of Science and Higher Education, as part of the project "*Support for the management of scientific research and commercialization of R&D results in research units and enterprises*" (POIR 2014–2020), and the Priority Research Area qLife under the program "Excellence Initiative Research University" at the Jagiellonian University in Krakow. W.Pietruś acknowledges the support of InterDokMed project no. POWR.03.02.00–00-I013. The authors thank Dr. Krzysztof Marciniec for performing HR-MS analyses. Special appreciations to Anna Chudzik and Natalia Kaczocha for their support in monoamine oxidase inhibition assays.

Appendix A. Supplementary data

Supplementary data to this article can be found online at https://doi.org/10.1016/j.ejmech.2022.114329.

References

[1] C. Binda, P. Newton-Vinson, F. Hubálek, D.E. Edmondson, A. Mattevi, Structure of human monoamine oxidase B, a drug target for the treatment of neurological disorders, Nat. Struct. Biol. 9 (1) (2002) 22–26.

[2] R.R. Ramsay, Molecular aspects of monoamine oxidase B, Prog. Neuro-Psychopharmacol. Biol. Psychiatry 69 (2016) 81–89.

[3] J.K. Mallajosyula, D. Kaur, S.J. Chinta, S. Rajagopalan, A. Rane, D.G. Nicholls, D.A. Di Monte, H. Macarthur, J.K. Andersen, MAO-B Elevation in mouse brain astrocytes results in Parkinson's pathology, PLoS One 3 (2008), e1616.

[4] M.B.H. Youdim, Y.S. Bakhle, Monoamine oxidase: isoforms and inhibitors in Parkinson's disease and depressive illness, Br. J. Pharmacol. 147 (Suppl 1) (2006) S287–S296. Suppl.

[5] N.T. Tzvetkov, H.G. Stammler, B. Neumann, S. Hristova, L. Antonov, M. Gastreich, Crystal structures, binding onteractions, and ADME evaluation of brain penetrant N-substituted indazole-5-carboxamides as subnanomolar, selective monoamine oxidase B and dual MAO-A/B inhibitors, Eur. J. Med. Chem. 127 (2017) 470–492.

[6] S. Manzoor, N. Hoda, A Comprehensive review of monoamine oxidase inhibitors as anti-Alzheimer's disease agents: a review, Eur. J. Med. Chem. 206 (2020) 112787.

[7] E. Borroni, B. Bohrmann, F. Grueninger, E. Prinssen, S. Nave, H. Loetscher, S.J. Chinta, S. Rajagopalan, A. Rane, A. Siddiqui, B. Ellenbroek, J. Messer, A. Pähler, J.K. Andersen, R. Wyler, A.M. Cesura, Sembragiline: a novel, selective monoamine oxidase type B inhibitor for the treatment of Alzheimer's disease, J. Pharmacol. Exp. Therapeut. 362 (2017) 413–423.

[8] S. Schedin-Weiss, M. Inoue, L. Hromadkova, Y. Teranishi, N.G. Yamamoto, B. Wiehager, N. Bogdanovic, B. Winblad, A. Sandebring-Matton, S. Frykman, L.O. Tjernberg, Monoamine oxidase B is elevated in Alzheimer disease neurons, is associated with γ-secretase and regulates neuronal amyloid β-peptide levels, Alzheimer's Res. Ther. 9 (2017) 57.

[9] S.F. Carter, M. Schöll, O. Almkvist, A. Wall, H. Engler, B. Långström, A. Nordberg, Evidence for astrocytosis in prodromal Alzheimer disease provided by ^{11}C-deuterium-L-deprenyl: a multitracer PET paradigm combining ^{11}C-Pittsburgh compound B and ^{18}F-FDG, J. Nucl. Med. 53 (2012) 37–46.

[10] B.P. Kennedy, M.G. Ziegler, M. Alford, L.A. Hansen, L.J. Thal, E. Masliah, Early and persistent alterations in prefrontal cortex MAO A and B in Alzheimer's disease, J. Neural. Transm. 110 (2003) 789–801.

[11] B. Gulyás, E. Pavlova, P. Kása, K. Gulya, L. Bakota, S. Várszegi, E. Keller, M.C. Horváth, S. Nag, I. Hermecz, K. Magyar, C. Halldin, Activated MAO-B in the brain of Alzheimer patients, demonstrated by [^{11}C]-L-deprenyl using whole hemisphere autoradiography, Neurochem. Int. 58 (2011) 60–68.

[12] M. Sano, C. Ernesto, R.G. Thomas, M.R. Klauber, K. Schafer, M. Grundman, P. Woodbury, J. Growdon, C.W. Cotman, E. Pfeiffer, L.S. Schneider, L.J. Thal, A Controlled trial of selegiline, alpha-tocopherol, or both as treatment for Alzheimer's disease. The Alzheimer's disease cooperative study, N. Engl. J. Med. 336 (1997) 1216–1222.

[13] G.K. Wilcock, J. Birks, A. Whitehead, S.J.G. Evans, The effect of selegiline in the treatment of people with Alzheimer's disease: a meta-analysis of published trials, Int. J. Geriatr. Psychiatr. 17 (2002) 175–183.

[14] J.-H. Park, Y.H. Ju, J.W. Choi, H.J. Song, B.K. Jang, J. Woo, H. Chun, H.J. Kim, S.J. Shin, O. Yarishkin, S. Jo, M. Park, S.K. Yeon, S. Kim, J. Kim, M.-H. Nam, A.M. Londhe, J. Kim, S.J. Cho, S. Cho, C. Lee, S.Y. Hwang, S.W. Kim, S.-J. Oh, J. Cho, A.N. Pae, C.J. Lee, K.D. Park, Newly developed reversible MAO-B inhibitor circumvents the shortcomings of irreversible inhibitors in Alzheimer's disease, Sci. Adv. 5 (2019), eaav0316.

[15] A.S. Hogendorf, A. Hogendorf, R. Kurczab, J. Kalinowska-Tłuscik, P. Popik, A. Nikiforuk, M. Krawczyk, G. Satała, T. Lenda, J. Knutelska, R. Bugno, J. Staroń, W. Pietruś, M. Matıoka, K. Dubiel, R. Moszczynski-Petkowski, J. Pieczykolan, M. Wieczorek, B. Pilarski, P. Zajdel, A. Bojarski, J. 2-Aminoimidazole-based antagonists of the 5-HT$_6$ receptor - a new concept in aminergic GPCR ligand design, Eur. J. Med. Chem. 179 (2019) 1–15.

[16] K. Grychowska, G. Satała, T. Kos, A. Partyka, E. Colacino, S. Chaumont-Dubel, X. Bantreil, A. Wesołowska, M. Pawłowski, J. Martinez, P. Marin, G. Subra, A.J. Bojarski, F. Lamaty, P. Popik, P. Zajdel, Novel 1*H*-pyrrolo[3,2-*c*]quinoline based 5-HT$_6$ receptor antagonists with potential application for the treatment of cognitive disorders associated with Alzheimer's disease, ACS Chem. Neurosci. 7 (2016) 972–983.

[17] K. Grychowska, S. Chaumont-Dubel, R. Kurczab, P. Koczurkiewicz, C. Deville, M. Krawczyk, W. Pietruś, G. Satała, S. Buda, K. Piska, M. Drop, X. Bantreil, F. Lamaty, E. Pękala, A.J. Bojarski, P. Popik, P. Marin, P. Zajdel, Dual 5-HT$_6$ and D$_3$ receptor antagonists in a group of 1*H*-pyrrolo[3,2-*c*]quinolines with neuroprotective and procognitive activity, ACS Chem. Neurosci. 10 (2019) 3183–3196.

[18] P. Zajdel, K. Grychowska, S. Mogilski, R. Kurczab, G. Satała, R. Bugno, T. Kos, J. Gołębiowska, N. Malikowska-Racia, A. Nikiforuk, S. Chaumont-Dubel, X. Bantreil, M. Pawłowski, J. Martinez, G. Subra, F. Lamaty, P. Marin, A.J. Bojarski, P. Popik, Structure-based design and optimization of FPPQ, a dual-acting 5-HT$_3$ and 5-HT$_6$ receptor antagonist with antipsychotic and procognitive properties, J. Med. Chem. 64 (2021) 13279–13298.

[19] M. Drop, X. Bantreil, K. Grychowska, G.U. Mahoro, E. Colacino, M. Pawłowski, J. Martinez, G. Subra, P. Zajdel, F. Lamaty, Continuous flow ring-closing metathesis, an environmentally-friendly route to 2,5-dihydro-1*H*-pyrrole-3-carboxylates, Green Chem. 19 (2017) 1647–1652.

[20] C.G. Neochoritis, T. Zarganes-Tzitzikas, S. Stotani, A. Dömling, E. Herdtweck, K. Khoury, A. Dömling, Leuckart-Wallach route toward isocyanides and some applications, ACS Comb. Sci. 17 (2015) 493–499.

[21] K. Grychowska, B. Kubica, M. Drop, E. Colacino, X. Bantreil, M. Pawłowski, J. Martinez, G. Subra, P. Zajdel, F. Lamaty, Application of the ring-closing metathesis to the formation of 2-aryl-1*H*-pyrrole-3-carboxylates as building blocks for biologically active compounds, Tetrahedron 72 (2016) 7462–7469.

[22] A. Garrido, I. Lepailleur, S.M. Mignani, P. Dallemagne, C. Rochais, hERG Toxicity assessment: useful guidelines for drug design, Eur. J. Med. Chem. 195 (2020) 112290.

[23] B.M. Johnson, Y.-Z. Shu, X. Zhuo, N.A. Meanwell, Metabolic and pharmaceutical aspects of fluorinated compounds, J. Med. Chem. 63 (2020) 6315–6386.

[24] M. Morari, A. Brugnoli, C.A. Pisanò, S. Novello, C. Caccia, E. Melloni, G. Padoani, S. Vailati, M. Sardina, Safinamide differentially modulates in vivo glutamate and GABA release in the rat hippocampus and basal ganglia, J. Pharmacol. Exp. Therapeut. 364 (2018) 198–206.

[25] R. Wang, P.H. Reddy, Role of glutamate and NMDA receptors in Alzheimer's disease, J. Alzheimers. Dis. 57 (2017) 1041–1048.

[26] P. Zajdel, M. Bednarski, J. Sapa, G. Nowak, Ergotamine and nicergoline — facts and myths, Pharmacol. Rep. 67 (2015) 360–363.

[27] A. Więckowska, N. Szałaj, I. Góral, A. Bucki, G. Latacz, K. Kiec-Kononowicz, Ò.M. Bautista-Aguilera, A. Romero, E. Ramos, J. Egea, V. Farré Alíns, Á. González-Rodríguez, F. López-Muñoz, M. Chioua, J. Marco-Contelles, In vitro and in silico ADME-Tox profiling and safety significance of multifunctional monoamine oxidase inhibitors targeting neurodegenerative diseases, ACS Chem. Neurosci. 11 (2020) 3793–3801.

[28] C.J. Garwood, L.E. Ratcliffe, J.E. Simpson, P.R. Heath, P.G. Ince, S.B. Wharton, Review: astrocytes in Alzheimer's disease and other age-associated dementias: a supporting player with a central role, Neuropathol. Appl. Neurobiol. 43 (2017) 281–298.

[29] R.E. González-Reyes, M.O. Nava-Mesa, K. Vargas-Sánchez, D. Ariza-Salamanca, L. Mora-Muñoz, Involvement of astrocytes in Alzheimer's disease from a neuroinflammatory and oxidative stress perspective, Front. Mol. Neurosci. 10 (2017) 427.

[30] A. Ennaceur, J. Delacour, A new one-trial test for neurobiological studies of memory in rats. 1: behavioral data, Behav. Brain Res. 31 (1988) 47–59.

[31] Y. Kitamura, K. Kitagawa, S. Kimoto, H. Sagara, K. Shibata, H. Kawasaki, T. Sendo, Y. Gomita, Selegilin exerts antidepressant-like effects during the forced swim test in adrenocorticotropic hormone-treated rats, J. Pharmacol. Sci. 106 (2008) 639–644.

[32] T. Ishikawa, M. Okano, A. Minami, H. Tsunekawa, H. Satoyoshi, Y. Tsukamoto, K. Takahata, S. Muraoka, Selegiline ameliorates depression-like behaviors in rodents and modulates hippocampal dopaminergic transmission and synaptic plasticity, Behav. Brain Res. 359 (2019) 353–361.

[33] T. Sunderland, R.M. Cohen, S. Molchan, B.A. Lawlor, A.M. Mellow, P.A. Newhouse, P.N. Tariot, E.A. Mueller, D.L. Murphy, High-dose selegiline in treatment-resistant older depressive patients, Arch. Gen. Psychiatr. 51 (1994) 607–615.

[34] E. Peña, C. Borrué, M. Mata, J.C. Martínez-Castrillo, A. Alonso-Canovas, J.L. Chico, L. López-Manzanares, M. Llanero, J. Herreros-Rodríguez, A. Esquivel, T. Maycas-Cepeda, C. Ruíz-Huete, Impact of SAfinamide on depressive symptoms in Parkinson's disease patients (SADness-PD study): a multicenter retrospective study, Brain Sci. (2021) 11.

[35] C.M. Labandeira, M.G. Alonso Losada, R. Yáñez Baña, M.I. Cimas Hernando, I. Cabo López, J.M. Paz González, M.J. Gonzalez Palmás, C. Martínez Miró, D. Santos García, Effectiveness of safinamide over mood in Parkinson's disease patients: secondary analysis of the open-label study SAFINONMOTOR, Adv. Ther. 38 (2021) 5398–5411.

[36] P. Pérez-Torre, J.L. López-Sendón, V. Mañanes Barral, I. Parees, S. Fanjul-Arbós, E. Monreal, A. Alonso-Canovas, J.C. Martínez Castrillo, Concomitant treatment with safinamide and antidepressant drugs: safety data from real clinical practice, Neurologia (2021), https://doi.org/10.1016/j.nrl.2021.08.004. In press.

[37] C. Binda, J. Wang, L. Pisani, C. Caccia, A. Carotti, P. Salvati, D.E. Edmondson, A. Mattevi, Structures of human monoamine oxidase B complexes with selective noncovalent inhibitors: safinamide and coumarin analogs, J. Med. Chem. 50 (2007) 5848–5852.

[38] J. Reis, N. Manzella, F. Cagide, J. Mialet-Perez, E. Uriarte, A. Parini, F. Borges, C. Binda, Tight-binding inhibition of human monoamine oxidase B by chromone analogs: a kinetic, crystallographic, and biological analysis, J. Med. Chem. 61 (2018) 4203–4212.

[39] H. Berman, K. Henrick, H. Nakamura, Announcing the Worldwide protein data bank, United States, Nat. Struct. Biol. (December 2003) 980.

[40] T. Halgren, New method for fast and accurate binding-site identification and analysis, Chem. Biol. Drug Des. 69 (2007) 146–148.

[41] T.A. Halgren, Identifying and characterizing binding sites and assessing druggability, J. Chem. Inf. Model. 49 (2009) 377–389.

[42] LigPrep Version 3.6.

[43] J.R. Greenwood, D. Calkins, A.P. Sullivan, J.C. Shelley, Towards the comprehensive, rapid, and accurate prediction of the favorable tautomeric states of drug-like molecules in aqueous solution, J. Comput. Aided Mol. Des. 24 (2010) 591–604.

[44] J.C. Shelley, A. Cholleti, L.L. Frye, J.R. Greenwood, M.R. Timlin, M. Uchimaya, Epik: a software program for PKa prediction and protonation state generation for drug-like molecules, J. Comput. Aided Mol. Des. 21 (2007) 681–691.

[45] G.M. Sastry, M. Adzhigirey, T. Day, R. Annabhimoju, W. Sherman, Protein and ligand preparation: parameters, protocols, and influence on virtual screening enrichments, J. Comput. Aided Mol. Des. 27 (2013) 221–234.
[46] E. Harder, W. Damm, J. Maple, C. Wu, M. Reboul, J.Y. Xiang, L. Wang, D. Lupyan, M.K. Dahlgren, J.L. Knight, J.W. Kaus, D.S. Cerutti, G. Krilov, W.L. Jorgensen, R. Abel, R.A. Friesner, OPLS3 : a force field providing broad coverage of drug-like small molecules and proteins, J. Chem. Theor. Comput. 12 (2016) 281–296.
[47] D. Shivakumar, J. Williams, Y. Wu, W. Damm, J. Shelley, W. Sherman, Prediction of absolute solvation free energies using molecular dynamics free energy perturbation and the OPLS force field, J. Chem. Theor. Comput. 6 (2010) 1509–1519.
[48] W.L. Jorgensen, D.S. Maxwell, J. Tirado-Rives, Development and testing of the OPLS all-atom force field on conformational energetics and properties of organic liquids, J. Am. Chem. Soc. 118 (1996) 11225–11236.
[49] R.A. Friesner, J.L. Banks, R.B. Murphy, T.A. Halgren, J.J. Klicic, D.T. Mainz, M.P. Repasky, E.H. Knoll, M. Shelley, J.K. Perry, D.E. Shaw, P. Francis, P.S. Shenkin, Glide: a new approach for rapid, accurate docking and scoring. 1. Method and assessment of docking accuracy, J. Med. Chem. 47 (2004) 1739–1749.
[50] R.A. Friesner, R.B. Murphy, M.P. Repasky, L.L. Frye, J.R. Greenwood, T.A. Halgren, P.C. Sanschagrin, D.T. Mainz, Extra Precision Glide: docking and scoring incorporating a model of hydrophobic enclosure for protein-ligand complexes, J. Med. Chem. 49 (2006) 6177–6196.
[51] T.A. Halgren, R.B. Murphy, R.A. Friesner, H.S. Beard, L.L. Frye, W.T. Pollard, J.L. Banks, Glide: a new approach for rapid, accurate docking and scoring. 2. Enrichment factors in database screening, J. Med. Chem. 47 (2004) 1750–1759.
[52] A.E. Cho, V. Guallar, B.J. Berne, R. Friesner, Importance of accurate charges in molecular docking: quantum mechanical/molecular mechanical (QM/MM) approach, J. Comput. Chem. 26 (2005) 915–931.
[53] Y. Cheng, W.H. Prusoff, Relationship between the inhibition constant (K_1) and the concentration of inhibitor which causes 50 per cent inhibition (I_{50}) of an Enzymatic Reaction, Biochem. Pharmacol. 22 (1973) 3099–3108.
[54] A. Stössel, M. Schlenk, S. Hinz, P. Küppers, J. Heer, M. Gütschow, C.E. Müller, Dual targeting of adenosine A_{2A} receptors and monoamine oxidase B by 4*H*-3,1-benzothiazin-4-ones, J. Med. Chem. 56 (2013) 4580–4596.
[55] D. Łażewska, A. Olejarz-Maciej, D. Reiner, M. Kaleta, G. Latacz, M. Zygmunt, A. Dorož-Płonka, T. Karcz, A. Frank, H. Stark, K. Kieć-Kononowicz, Dual target ligands with 4-tert-butylphenoxy scaffold as histamine H_3 receptor antagonists and monoamine oxidase B inhibitors, Int. J. Mol. Sci. 21 (2020) 3411.
[56] N.T. Tzvetkov, S. Hinz, P. Küppers, M. Gastreich, C.E. Müller, Indazole- and indole-5-carboxamides: selective and reversible monoamine oxidase B inhibitors with subnanomolar potency, J. Med. Chem. 57 (2014) 6679–6703.
[57] D. Łażewska, A. Olejarz-Maciej, M. Kaleta, M. Bajda, A. Siwek, T. Karcz, A. Dorož-Płonka, U. Cichoń, K. Kuder, K. Kieć-Kononowicz, 4-Tert-pentylphenoxyalkyl derivatives - histamine H_3 receptor ligands and monoamine oxidase B inhibitors, Bioorg. Med. Chem. Lett 28 (2018) 3596–3600.
[58] R.A. Copeland, Evaluation of Enzyme Inhibitors in Drug Discovery. A Guide for Medicinal Chemists and Pharmacologists, John Wiley & Sons, Inc., Hoboken, N. J., 2005.
[59] J.K. Singh, A. Solanki, S.V. Shirsath, Comparative in vitro intrinsic clearance of imipramine in multispecies liver microsomes: human, rat, mouse and dog, J. Drug Metabol. Toxicol. 3 (2012) 126.
[60] V.N. Sumantran, Cellular chemosensitivity assays: an overview, Methods Mol. Biol. 731 (2011) 219–236.
[61] P. Popik, M. Holuj, A. Nikiforuk, T. Kos, R. Trullas, P. Skolnick, 1-Aminocyclopropanecarboxylic acid (ACPC) produces procognitive but not antipsychotic-like effects in rats, Psychopharmacology (Berl) 232 (2015) 1025–1038.
[62] R.D. Porsolt, A. Bertin, M. Jalfre, Behavioral despair in mice: a primary screening test for antidepressants, Arch. Int. Pharmacodyn. Ther. 229 (1977) 327–336.